AN ABSTRACT OF THE THESIS OF

Taylor A. Bates for the degree of Master of Science in Botany and Plant Pathology presented on June 3, 2021.

Title: Science Takes Flight: Detection of Black Leg on Turnip Gray Mold on Hemp.

Abstract approved:

_____

Cynthia M. Ocamb

Disease detection through traditional techniques such as scouting fields on foot, molecular assays, or morphological identification of plant pathogens is time consuming and costly. Disease diagnosis in the field can be extremely subjective, and largely depends on the experience and knowledge of pathogen identification and disease quantification. This thesis provides an evaluation of remote sensing for assessing disease in agricultural field settings via an unmanned aerial vehicle and machine learning. Case studies are presented on two different fungal diseases important in western Oregon crop production: black leg on turnip (incited by *Leptosphaeria* spp.) and gray mold on hemp (caused by *Botrytis* spp.). Both case studies utilized a support vector machine model to classify pixels of digital images collected with a multispectral Micasense RedEdge-M optical sensor. Turnip leaves were imaged at 1.5 m *in situ* while hemp plant images were collected by an unmanned aerial vehicle with flights at 10 m *ex situ*. Detection of pixels exemplifying black leg leaf spot symptoms on turnip leaves had an overall accuracy of 97.0% with a model sensitivity of 0.48. The support vector machine model utilized in gray mold detection on hemp incorporated a novel vegetation index, a modified green-red vegetation index along with the triangular greenness index, to identify pixels of diseased hemp inflorescences extracted from background soil and vegetation. The model had an overall accuracy of 95.8% when identifying a hemp inflorescence as

diseased or non-diseased. False negatives were found to be high with a sensitivity of 0.70 in the hemp model. Additionally, gray mold disease incidence determined using the support vector machine model was compared with disease assessments collected by scouting on foot and was found to have similar treatment rankings, although the differences in the relative percentages between the two methods were found to be large. The findings of this study provide the foundation for further development of remote sensing techniques for black leg disease assessments in *Brassica* crops and potential deployment of remote sensing strategies for measuring gray mold in hemp fields.

Science Takes Flight: Detection of Black Leg on Turnip and Gray Mold on Hemp

by
Taylor A. Bates

A THESIS

submitted to

Oregon State University

in partial fulfillment of
the requirements for the
degree of

Master of Science

Presented June 3, 2021
Commencement June 2021

Master of Science thesis of Taylor A. Bates presented on June 3, 2021

APPROVED:

Major Professor, representing Botany and Plant Pathology

Head of the Department of Botany and Plant Pathology

Dean of the Graduate School

I understand that my thesis will become part of the permanent collection of Oregon State University libraries. My signature below authorizes release of my thesis to any reader upon request.

Taylor A. Bates, Author

ACKNOWLEDGEMENTS

I would first like to thank my committee members, first and foremost, my major advisor, Dr. Cynthia Ocamb. This project would not have been possible without her support and scientific knowledge. I want to thank her for providing me with the opportunity to pursue my academic interests in my thesis work and the range of projects she allowed me to participate in.

I want to also thank Dr. David Gent for never denying statistical analysis advice even after he had explained it to me twice over. Also, for reviewing so many of my manuscripts, which always came out better after he got his hands on it.

Thanks to Dr. Kristie Buckland for providing the drone and camera to make this project possible. I would also like to thank Dr. Buckland's research associate, Dr. Ann Rasmussen, for meeting me at fields across the Willamette Valley and teaching me how to operate the drone, camera, and software.

I would like to thank Dr. Christopher Still for being my graduate representative council member and bringing a knowledge of remote sensing to my thesis work.

A big thanks to Dr. Bill Thomas for his humor, scientific knowledge, gracious personality, and his steady coffee pouring hand in the late afternoon.

I want to thank the undergraduates who helped whenever I provided an opportunity: Mariah Dietrich, Tim Flodquist, Alexa Montgomery, and Darby Bergyl.

I want to thank my family and friends for providing me the emotional support and sound logic to step back from research to enjoy all the other things life has to offer when I needed a break.

Finally, I would like to thank my fiancé, Ashley Brand, I could not have done this without here patience and love from the first day my graduate program started to the end.

CONTRIBUTION OF AUTHORS

Dr. Cynthia M. Ocamb assisted with project development and edited all manuscripts. Dr. David H. Gent assisted in statistical analysis for field-based findings and reviewed the manuscript. Dr. Kristine R. Buckland provided the hardware and software used in this project along with reviewing the manuscript. Dr. Ann Rasmussen provided training and assistance in unmanned aerial vehicle flights.

TABLE OF CONTENTS

TABLE OF CONTENTS (Continued)

Page

TABLE OF CONTENTS (Continued)

Page

LIST OF FIGURES

Figure Page

LIST OF FIGURES (Continued)

Figure Page

LIST OF TABLES

Table Page

Chapter 1: Introduction

After a brief overview of agricultural production in the Willamette Valley, two agricultural commodities in Oregon are reviewed, turnip grown for seed and hemp grown for its flowers. Additionally, two of the most devastating pathogens associated with these crops, black leg on turnip and gray mold on hemp, are also reviewed. Lastly, a short review of remote sensing use in agriculture and a case study for potential applications in the two host-pathogen systems is provided.

Agriculture in the Willamette Valley of Oregon

The Willamette Valley of western Oregon is home to over 100 different cultivated crops (USDA FSA 2020). Among those, *Brassica* crops, otherwise known as crucifers, make up a large portion of the seed crops cultivated in the valley. This valley region extends about 210 km in length, ranges from 40 to 65 km wide, and experiences cool, wet winters and warm, dry summers (Walsh et al. 2010). Laying in the rain shadow of the Oregon coastal range, the valley receives an average of 110 cm of precipitation annually, largely between the months of October and May (Walsh et al. 2010). Over the years, growers have expanded crop production throughout the valley and benefitted from its ideal growing conditions. Specialty seed produced in Oregon and Washington supplies around 25% of the world's market for *Brassica* seed (Inglis et al. 2013), and is one of the few locations in the world where high quality *Brassica* seed production can take place. The scarcity of summer rain and the relatively mild winters allows for the vernalization necessary for high quality specialty seed production of brassicas. While much of the seed is kept in or near its U.S. origin, Europe and Asia offer profitable markets for growers in Oregon. Before *Brassica* seed can be shipped overseas, seed quality must be tested to gain certification as disease-free for most markets, among other import/export testing requirements. Among the requirements, black leg-free seed is typically needed for international and domestic transport of *Brassica* seed. Disease management strategies are generally utilized in the Willamette Valley to reduce the likelihood of seedborne

diseases to ensure the greatest economic value of specialty seed crops. To prevent or limit diseases, early detection, informed sprays, and preventative measures are necessary to meet the demands and requirements of foreign and domestic regulations on *Brassica* seed produced in the valley. Common *Brassica* diseases in Oregon include clubroot (*Plasmodiophora brassicae*), downy mildew (*Peronospora parasitica*), powdery mildew (*Erysiphe polygoni*), Sclerotinia stem rot (*Sclerotinia sclerotiorum*), chlorotic leaf spot (*Pyrenopeziza brassicae*), black spot (*Alternaria brassicae*), white rust (*Albugo candida*), and black leg (*Leptosphaeria maculans* and *Leptosphaeria biglobosa*) (Pscheidt and Ocamb 2021).

Black leg

One of the pathogens that disrupts healthy growth of *Brassica* species in the Willamette Valley of Oregon and worldwide (Howlett et al. 2001) is the fungus that causes black leg. This fungal pathogen causes significant yield losses in canola (*Brassica napa*) production in Europe (Fitt et al. 2006), Australia (Khangura and Barbetti 2001), and North America (Markell et al. 2008; Del Rio et al. 2012; Nepal et al. 2014). Black leg hadn't been a major disease problem in the Pacific Northwest, but outbreaks were observed on specialty seed crops in the Willamette Valley beginning in 2014 (Ocamb et al. 2015). Black leg was reported on canola in North Dakota in 1991 (Lamey and Hershman 1993), in Idaho in 2011 (Agostini et al. 2013), and soon after in Washington state (Paulitz et al. 2017). The recent reports of *Leptosphaeria* species in the Willamette Valley of Oregon occurred on *Brassica* vegetable and seed crops as well as weeds and the restricted acreage in canola production. Although this disease is widely regarded for its impact on canola due to large-scale production of canola across the world, black leg has even greater impact on many Brassicaceae crops including turnip (*Brassica rapa*) and radish (*Raphanus raphanistrum*) grown for seed, and also occurs on weedy *Brassica* species in the Willamette Valley of Oregon (Claassen et al. 2015). There are two fungal species known to cause black leg, *Leptosphaeria maculans* and *L. biglobosa*. This crucifer

disease, black leg, should not be confused as the potato bacterial disease caused by *Pectobacterium atrosepticum,* commonly referred to as blackleg. Recent studies have placed these *Leptosphaeria* species in the *Plenodomus* genus (De Gruyter et al. 2013), where the teleomorph *L. maculans* is now a synonym of *Plenodomus lingam* and the anamorph is *Phoma lingam*. Similarly, the teleomorph *L. biglobosa,* is now referred to as *Plenodomus biglobosus* with an unnamed anamorph. While much of the crop failure in canola has been associated with *L. maculans* (Markell et al. 2008), both species are found in the Willamette Valley and seem to be of similar destructive consequence. The two closely related pathogens are considered a species complex and can oftentimes be found occurring together (Mendes-Pereira et al. 2003; Dilmaghani et al. 2009).

Black leg symptoms and disease biology

Leptosphaeria species produce both initial (primary) inoculum as well as secondary inoculum. The primary inoculum is derived from the over-summering/wintering or host-free period survival structures, and initiates infection during the next cropping cycle. Secondary inoculum is the inoculum generated after the first infection event takes place. The spore-bearing survival structure of *L. maculans* and *L. biglobosa* is a pseudothecium, which gives rise to sexual spores known as ascospores. Generally, *Leptosphaeria* will produce pseudothecia on infected crop residue, which provides the source of primary inoculum during the fall, winter, and spring in the Pacific Northwest. The mature ascospores are forcefully ejected from asci located inside the pseudothecia found on crop residues and are dispersed broadly across the landscape by wind (West et al. 2001). Ascospore release is associated with dry intervals within rainy periods, which commonly occurs during Oregon's autumn and winter, and ascospores can persist after release from the pseudothecium for up to 6 weeks (West et al. 1999). Infected canola residues have been shown to remain infectious for longer than 24 months in western Oregon (Berry 2019). *Leptosphaeria*-infected seeds may also act as an inoculum source (Rimmer

and Van de Berg 2007), but this is generally a less common occurrence when certified *Leptosphaeria*-free seed requirements are followed (West et al. 2001). A third source of primary inoculum comes from Brassicaceae weeds such birdsrape mustard, black mustard, wild radish, and others (Claassen et al. 2015). Fields within close proximity to Brassicaceae weeds are at risk for black leg due to the frequency of infected weed plants (Claassen 2016).

Secondary disease spread occurs on overwintered *Brassicas* with the production of asexual pycnidiospores (conidia) by pycnidia. Pycnidia appear as tiny black spots on foliar lesions or stem cankers (Fig. 1.1 B). The conidia typically do not travel more than one meter upon splash-dispersal (Hall et al. 1996), while the ascospores are reported to have traveled 500 meters from infected residues (West et al. 2001). Germinating spores typically infect through stomata or wounded tissues of the plant and have not been reported to infect via direct penetration of the cuticle (Sprague et al. 2007). Upon infection, hyphae can grow through vascular bundles of the xylem vessels or between parenchyma cells along the xylem and in the cortex, extending down into the basal region of the stem where the pathogen can remain symptomless (Sexton and Howlett 2001; Rouxel and Balesdent 2005). Small, light colored lesions develop on leaves and expand to about 2 cm in size, and the centers may hole punch (shothole effect) from the force of water droplets hitting the necrotic tissue in the center of leaf lesions (Figure 1.1) (West et al. 2001). As the spores inside the pycnidia mature and environmental conditions are met, conidia 3 to 5 μm by 1.5 to 2 μm in size will discharge in a column of light pinkish to purplish to white colored ooze called cirrhus (Ghanbarnia et al. 2011). Conidia are generally transmitted through splashing water droplets and are viable for up to 10 days (Li et al. 2007). The conidia incite secondary infections and further the spread of disease within a field. In Canada, black leg has developed in the field in the absence of ascospore showers, suggesting pycnidiospores may act as the main source of inoculum under some conditions (Ghanbarnia et al. 2011). In addition to leaf spots, gray to brown, oval-shaped lesions may present themselves on the stems and storage roots of susceptible plants. If canola and turnip are seriously compromised by stem infections, cankers

can lead to girdling of the plant and lodging. Because the black leg fungus grows systemically, seed pod infection can result in contaminated or infected seed (West et al. 2001). Although this disease has been referred to as monocyclic in Europe (West et al. 2001) and Australia (Li et al. 2007), the Willamette Valley in western Oregon experiences a polycyclic disease cycle, increasing the destructiveness of this pathogen.

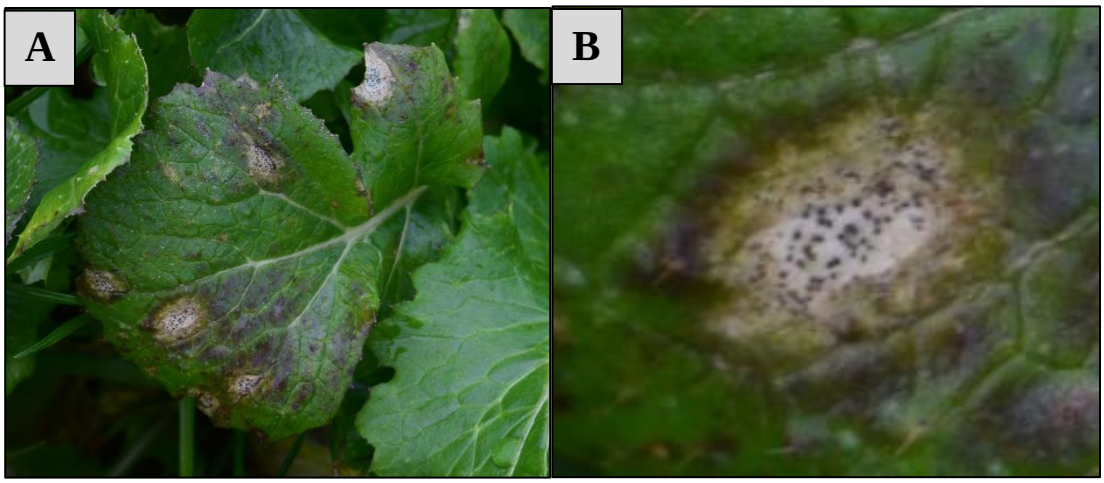

Figure 1.1 Turnip leaf displaying black leg leaf lesions as a result of infection by *Leptosphaeria* (A). Stereoscopic view of a leaf lesion with small black pycnidia (B).

The fall through spring rainfall in the Willamette Valley can exceed 100 cm during most years (Walsh et al. 2010), providing the cool, moist conditions for sporulation and infection by the fungus causing black leg. Around 8 to 72 hours of leaf wetness duration and 8 to 24°C can lead to leaf spot development, with 48 hours at 20°C resulting in the greatest number of leaf spot lesions (Biddulph et al. 1999). Huang et al. (2005) reported that development of black leg was different among countries, based on weather patterns. Aggressiveness of *Leptosphaeria* can vary depending on host crop, cultivar, weather, species, and strain of *Leptosphaeria*.

Black leg management

Cultural management practices

The best practices for disease suppression or elimination typically start with good cultural management. It is suggested to practice a four-year crop rotation before sowing another plant species susceptible to *Leptosphaeria* (West et al. 2001; Guo et al. 2005). This recommendation comes at the understanding that crop residue may harbor pseudothecia over three years, with the ascospore-bearing structure count diminishing greatly after this period. Crop residues are managed with different techniques among countries and depend on grower preferences. Countries such as India and China, which typically plant rice after a canola, tend to remove the entire canola plant from the field (West et al. 2000). This requires extra efforts from the growers but is good practice in diminishing the source of inoculum as well as following the practice of crop rotations. This may account for the absence of *L. maculans* in China, although a less aggressive *L. biglobosa* population does occur. Growers in other countries practice deep tillage and bury the crop residues underground. This can be damaging to the soil structure but is preferred over shallow tillage or no-till in regard to black leg management (Gladders and Musa 1980). Deep tillage also helps in combating volunteers of shattered seed from previous seasons in comparison to shallow tillage.

Field proximity to other susceptible crop fields previously planted is another important cultural management consideration. Conidia typically travel no more than a few meters, whereas ascospores likely don't travel more than a few kilometers. In terms of field-to-field transfer of the pathogen, ascospores are generally regarded as the primary concern where infected crop residues may exist. A separation of 500 meters between *Brassica* residues and new crops has been accepted amongst growers and researchers alike (West et al. 2001). Despite these distances traveled, ascospores are thought to travel distances greater than 500 meters, and subsequently, 500 meters should be considered a minimum distance and not an absolute when it comes to field protection (West et al. 2001).

Other cultural control recommendations include planting later in the spring or earlier in the fall when conditions are not as conducive for black leg in the Pacific Northwest. Additionally, awareness of mechanical spread of the disease when using equipment in an infected field, ensuring equipment is properly cleaned before working in another field, or avoided all together will help control disease spread. Because black leg is capable of growing on many crucifer crops, control of weedy *Brassica* species nearby which may harbor the disease is also important. For organic production, simply removing infected leaves or infected plants is also helpful in slowing the spread of disease.

Chemical control practices

A number of chemicals can be used to control black leg, but eradication through chemical treatment is not likely. Canola plants tend to be more susceptible to disease during the early stages of growth rather than more mature plants (Ghanbarnia et al. 2011). Mature canola plants may outgrow the disease and tend to be less susceptible to infection. Although it can be burdensome and financially difficult to cover the costs of preventative fungicide applications, black leg is best treated early with fungicides, and prior to infection. Because younger plants are more susceptible and timing is noted to be of great importance with black leg management, fungicide applications should be conducted not later than the first two months after germination (West et al. 1999). Later fungicide sprays are almost unnecessary in canola because the fungicides are not designed for eradication, nor do they offer significant kick-back effects. Once the pathogen has reached the stem, current fungicides registered for canola do not further control the disease, thus the need to protect leaves from initial infections and to spray early rather than later in plant development (Gladders et al. 1998). Another step to black leg management is using treated seed. In the U.S. Pacific Northwest region, thiabendazole (Mertect 340-F) and iprodione (Rovral 4F) are registered as seed treatments for turnip and other *Brassica* crops (Pscheidt and Ocamb 2021).

The foliar fungicides registered for management of black leg in turnip in Oregon include pyraclostrobin (Cabrio EG), prothioconazole (Proline 480 SC), and azoxystrobin (Quadris Flowable) (Pscheidt and Ocamb 2021). There are additional fungicides that are registered in Oregon for black leg management in canola and other Brassicaceae crops. When determining the best time to apply fungicides, four agronomic factors should be considered: cultivar susceptibility, soil type, plant growth stage, and plant vigor (West et al. 2001). In the Willamette Valley, the crop type (vegetable vs. vegetable seed crop vs. canola grown for oilseed) is a critical consideration for timing of fungicide applications, both the onset of the first application and intervals of protective sprays.

Host resistance and biological control practices

Different biological control agents have been explored with limited success for black leg management. Fungi that break down plant residue have been effective in lowering black leg fungal populations as well as the application of a bacterium with known antifungal properties (West et al. 2001). Prior to any fungicide applications, canola seed lines should be selected from germplasm which contains at least some resistance to the pathogen, and seed should be certified as free of *Leptosphaeria*. Breeding programs seeking R-genes in canola have been underway for years. Acquiring novel canola lines with known resistance is a crucial step in combating black leg in the field. Additionally, new canola lines that are genetically modified are produced every few years and provide the grower greater control over their field. These plant lines may contain resistance to highly-effective fungicides which could not be used otherwise, as well as the input of R-genes that impart some level of resistance to *Leptosphaeria*. Overcoming major gene (R-genes) resistance is of great concern due to the constant pathogen selection that occurs with sexual recombination (ascospores) in the field, thus demanding continuous cultivar development (Howlett et al. 2001). In Australia, single R-gene resistance appears to break down in 3 to 4 years. Kutcher et al. (2011) suggest an integrated approach that combines multiple strategies in concert rather than reliance on a single strategy for providing the best

management of black leg. These recommendations outlined in this chapter are not all-inclusive, nor provide all the tools growers have access to or everything that has been reported as effective. Awareness of disease threats and regular scouting of *Brassica* fields for black leg will allow for the timeliest decisions and help crop experts and growers to make the soundest management decisions.

The reemergence of hemp production in the U.S.

After decades of legislative restrictions on the cultivation of *Cannabis* in the United States, legislation passed by the federal government has now led to the reemergence of the hemp industry. While *Cannabis* production may now be more mainstream than it has anytime in the past century, this crop has been cultivated by humans for thousands of years. Research suggests that *Cannabis* and *Humulus* diverged about 27.8 million years ago, with the center of origin for *Cannabis* possibly near Qinghai Lake on the northeastern Tibetan Plateau (McPartland et al. 2019). Evidence of *Cannabis* first being used by humans goes back 10,000 years to its utility in Japan as a food source (McPartland et al 2019). Kraezel et al. (1998) suggests *Cannabis* may have been used roughly 12,000 years ago in Central Asia, where relics of sand pottery with hempen cord fiber along the surface were recovered. Others suggest it was not until 5,600 years ago in China that hemp fiber was first used for silk and spinning wheels (McPartland et al. 2019). Documented use of *Cannabis* sacramentally dates back 2,500 years ago with evidence discovered in the Jiaya tomb of a Chinese male in modern northwest China (Jiang et al. 2006; Jiang et al. 2016). While many of these origins are still under debate, the cultivation and uses of *Cannabis* are known to be ancient and among the first crops cultivated by humans.

Hemp taxonomy

Cannabis sativa L. was first described by the “father” of taxonomy, Carl Linnaeus. At the time, Linnaeus was unaware of the types found in Asia and India

and thus, classified *C. sativa* as the sole species of the genus in 1753 (McPartland 2017). In Europe, *C. sativa* was cultivated as a fiber crop, distinct from the medicinal *Cannabis* found in both India and Asia (Hartsel et al. 2016). Jean-Baptiste Lamarck, another well-known taxonomist of the time, recognized the differences in plant size, shape, leaf structure, and psychoactive effects associated with those found in India and Asia. This ultimately led him to create a separate species in 1785 that was reported as *Cannabis indica* (McPartland 2017). Over a century later, a third *Cannabis* species was named by a Soviet botanist, D.E. Janischevsky. In Soviet Russia, a shorter auto-flowering variety was named *Cannabis ruderalis*, becoming the third member of this genus (McPartland 2018). There is still controversy concerning the taxonomy of these three species. The two dominating schools of thought are split between monotypic and polytypic position (Hartsel et al. 2016). Many botanists believe that all *Cannabis* species are *C. sativa* because the three are often interbred to generate unique phenotypes. This would therefore support the biological species concept making them one species and three separate varieties or subspecies with unique phenotypes. Alternatively, Sawler et al. (2015) conducted a genome-wide analyses using 14,000 SNPs on 81 marijuana and 43 hemp lines or strains and demonstrated that enough genotypic distinction exists between *C. sativa* and *C. indica* to classify the two as individual species. While this debate is still ongoing, in this thesis, the polytypic nomenclature is used unless distinguished otherwise.

Hemp biology

Cannabis is dioecious, but under stressful environmental conditions, typically from artificial changes in the light cycle, may cause the plant to become hermaphroditic, leading to a monoecious plant. Generally, the female plants are much rounder and bushier while the males are tall and slim (Raman et al. 2017). While this dioecious growth pattern is a generalization, growth patterns of hemp are largely dictated by environment and cultivar selection as either fiber, seed, or medicinal type. The fiber cultivars are most often *C. sativa*-dominate strains while medicinal types

favor *C. indica* genetics. Most cultivars grown today are not true *C. sativa*, *C. indica*, or *C. ruderalis*, but are crosses between members of these three species. Despite this, there are known morphological differences between *C. sativa*, *C. indica*, and *C. ruderalis* which have been described by Anderson (1974), and draws distinctions defined by woody tissue anatomy. But as previously remarked, cultivars of today are a melting pot of the three-wild type varieties and/or species, and original wild-type species are believed to have been lost. Hemp cultivars used for fiber are generally taller in height and have a narrower canopy than the medicinal types grown for the chemical content of their flowers, which have a 'Christmas tree' appearance to them. Leaves are alternate or opposite in position on the stem, palmately compound or more recently termed, actinodromous, with 3 to 11 leaflets (Jiang et al. 2006; Chandra et al. 2017). The center leaflet is typically largest in size and lanceolate in shape with serrate margins and pinnate venation. Leaflets become more linear the further they extend from the center leaflet, but margins and venation remain the same. Adaxial surface ranges from a lighter pale green to dark green, depending on leaf age, with cystolith non-glandular trichomes while the abaxial surface is much lighter in color with a whitish-green appearance and capitate-sessile glandular trichomes and non-glandular covering trichomes (Raman et al. 2019). Flower formation occurs at the nodes where the leaf petioles meet the stem and the female or male reproductive organs are found. The stigma will begin to form a 'pre-flower' early in the bloom period and continuously grows to form a 'bud'. The collection of buds on a hemp stalk or stem is referred to as a 'cola' or inflorescence. Hemp seeds are smooth and spherical with color being light brown to dark gray and often times a mottled appearance (Ehrensing 1998). Seeds are 2.5 to 4 mm in diameter and 3 to 6 mm in length (Dewey 1913), weighing on average 16 grams, but can be much smaller or larger (Dempsey 1975). Additional morphological characterization of *Cannabis* species and anatomy can be found in Chandra et al. (2017).

Modern hemp history

While China was the major producer of hemp early on, hemp eventually became a cash crop in Europe during the 1500's due to its versatility as a fiber and for the high nutrient content found within its seeds (Johnson 1999). Despite widespread hemp production across Scotland, England, Wales, and Ireland in the following centuries, hemp demands could not be entirely met (Gibson 2006). This void was filled by Russia, who became the premier producer of hemp-based products and its number one agricultural exporter (Fortenbery and Mick 2014). With its noticeable strength and resistance to corrosion from saltwater, hemp was commonly used in seafaring vessel mast-cloth and rope construction. The use of hemp-fiber for military might allowed Italy to create one of the greatest naval fleets of the 1700's, during a period when it had the highest quality hemp cultivars (Kraenzel et al. 1998). This came prior to England's naval dominance that was largely attributed to hemp fiber as well (Fortenbery and Mick 2014). With the colonization of America and its close ties with European heritage, hemp was introduced to America and cultivated for fiber in 1645 (USDA ERS 2000).

Despite many years of stigma accompanied by a ban on production, people across America still remember its importance during America's early years. Hemp was reportedly used for cordage, sailcloth, uniforms, the first U.S. flag, drafting of the Declaration of Independence, and was even cultivated by the U.S. presidents Washington and Jefferson (Kraenzel et al. 1998; Fortenbery and Mick 2014). The hemp industry boomed during the mid-1800's, primarily in Kentucky but also in Missouri and Illinois. By the end of that century, the relevance of hemp began to shrink largely due to the cotton gin's ability to separate seed from cotton fibers along with the steam-powered engines taking over transportation markets. While many of the U.S. states attempted to cultivate hemp, essentially all production took place in Kentucky from the end of the Civil War to 1912 (Wright 1918). In 1913, the U.S production of hemp came to a halt, despite the fact that production was already dwindling, as the Marijuana Tax Act was imposed that gave the U.S. Treasury

Department oversight of its production. This tax was chiefly put in place as an attempt to prohibit production of *Cannabis* strains that were high in THC content (Ehrensing 1998). There was a slight resurgence in hemp production during WWII when both jute and abaca supplies were disrupted and roughly 13 U.S. states began growing hemp to help meet demands for fiber (Wright 1918; Dempsey 1975). While Oregon is now one of the nation's leaders in hemp production, commercial production never occurred during the state's early years. However, Ehrensing (1998) remarks that experimental crops were planted in the 1930's for a fiber crop trial conducted by the USDA and a hemp breeding program in Corvallis, Oregon was established, but soon after was transferred to Wisconsin. Recently, hemp cultivation has found much stronger footing in the state of Oregon.

Uses and economics of hemp

Hemp is said to have over 50,000 different uses, which suggests it could have large financial impacts on the world economy (Carus and Sarmento 2016). Estimates of hemp product sales and as a state-to-state commodity are difficult to measure due to the lack of data collection by USDA National Agricultural Statistics Service. States like Oregon are said to be in the top five in terms of hemp acreage in an almost billion-dollar national industry projected to reach almost $2 billion USD by 2022 (Smith 2019).

The three categories that encompass hemp uses include fiber, seed, and oil. While hemp-fiber was once in great demand, driving early hemp cultivation, hemp fiber has become less relevant today as alternatives such as flax, cotton, and synthetic fibers hold a production and cost-effective advantage. In 1999, hemp fiber only held 0.3% of the world fiber market demand (Cherney and Small 2016). From 1982 to 2002, the European Union (E.U.) subsidized hemp and flax harvesting and processing technologies with millions of dollars, giving them a share in the hemp fiber market (Small and Marcus 2002). The largest current supplier of hemp fiber is China; cheap

labor and a developed industry have made this market very difficult to compete with. The fiber in hemp is bast fiber, which is found between the phloem and bark. Primary uses include textiles, plastic composites, pulp for paper, building materials, and animal bedding (Small and Marcus 2002). The U.S. imported about $10 million (USD) worth of hemp fiber in 2013 (Fortenbery and Mick 2014), which was slightly down from the preceding three years. For the most part, the hemp fiber industry has been stable during the past 20 years. The hemp seed, oil, and oilcake industries have seen a large increase in production in Europe and Canada but little production in the U.S. and thus the U.S. requires importation to meet consumer demands (Cherney and Small 2016).

Hemp grown for seed holds promise for North American farmers. In 2013, there was roughly $85 million USD worth of hemp seed oil and oilcake imported into the U.S. (Fortenbery and Mick 2014). Hemp seed is generally used as food for both humans and livestock. It is also popular for edible oil and personal care products like soaps, shampoos, perfumes, etc. One of the advantages of oil derived from hemp seed is that new technologies are not required for processing. Machinery used for other oil seed crops' extractions have been shown to be effective for hemp seed oil extraction and is one of the reasons hemp oilseed production is more economically feasible in the U.S. compared to hemp fiber. There are also restrictions on the intercontinental shipment of seed from places like China and the E.U. into the U.S. and coupled with the seed certification and the chance of the product going rancid, makes it a challenge for foreign producers to penetrate the U.S. hemp seed market.

Finally, oils extracted from the glandular trichomes contained in the flowers have become the primary target for the U.S. hemp industry of late. The compounds of hemp most sought after are cannabidiol (CBD) and more recently, cannabigerol (CBG). While there are already many useful chemical compounds found in the trichomes of hemp, more continue to be discovered as potential sources of valuable cosmetic, dietary, and health products. Hemp Business Journal estimates in 2017 that 23% of hemp sales came from CBD, 22% from personal care, 18% for industrial

applications, and 17% for food products (Smith 2019). This article also estimates that just under 35% of future hemp sales will go towards CBD in 2022. The future of hemp production in the Pacific Northwest is anticipated to predominantly revolve around the CBD market, along with other chemical compounds found in the trichomes of *Cannabis* flowers.

Hemp laws and regulations

Oregon lawmakers signed off on industrial hemp in 2009 by the approval of SB 676 but hemp production would have to wait a bit longer for the federal government to agree to the legalization of hemp production with the approval of the 2014 and 2018 Farm Bills. In 2014, the Federal Agricultural Act of 2014, commonly referred to as the 2014 Farm Bill (Jeliazkov et al. 2019), allowed for state pilot programs to begin cultivation of industrial hemp by both commercial growers and universities. Oregon's statewide hemp program was established soon after in 2015, guided by the 2014 Farm Bill. With the success of the 2014 Farm Bill and need for further legislation, another act was passed into law by the U.S. government in 2018. The Agriculture Improvement Act of 2018, commonly referred to as the 2018 Farm Bill, addressed commercial cultivation of industrial hemp and designated the USDA Agricultural Marketing Service to develop regulations (Jeliazkov et al. 2019). The interim rules for hemp production were released by the USDA on October 29, 2019. On January 15, 2021, the USDA published a final rule on the regulation covering the production of hemp in the U.S., which built on the rules set in October 2019 and were to take effect on March 22, 2021 (USDA AMS 2020). While laws and regulations may be changing in the coming years as new, improved legislation for the U.S. and Oregon is put into effect, there are no current signs that the hemp industry will imminently slow down.

Due to its high market value, hemp production acreage has increased rapidly since the inception of the 2014 Farm Bill. During 2018, Oregon had 584 registered

growers and 1441 registered grow locations (ODA 2020). This increased during 2019 to 1960 growers and 6040 registered grow sites. While the numbers have not been released for 2020 or 2021, production appears to be escalating in Oregon. The Oregon Department of Agriculture statistics show that as of August 21, 2020, over 25,000 acres of outdoor industrial hemp were registered for production (Jones 2020). Although the market is still stabilizing, hemp provides a potentially valuable crop for many farmers throughout Oregon.

While Oregon was one of the first states to legalize cultivation of hemp, its success and high demand has spurred many other states to follow suit. As of December 15, 2020, every continental state except for Idaho and Mississippi allows the cultivation of hemp for commercial, research, or pilot programs. With the 2018 Farm Bill and the removal of hemp from the Controlled Substances Act, researchers are now realizing the many research opportunities that this crop presents.

Diseases affecting hemp

In hemp disease reviews by McPartland (1996) and McPartland et al. (2000), 88 species of fungi were reported to attack *C. sativa* while more than 100 are listed by Farr and Rossman (2021). The numbers reported by McPartland occurred during a period when production of *Cannabis* was largely illegal across the world and little to no research was conducted tracing the plant health related issues. Now that *Cannabis* has taken a more global stage, with legalization seen not only across the U.S. but many places across the world, it is likely that the estimated number of pathogens infecting *Cannabis* will increase as more time passes.

Pathogens of *Cannabis* are beginning to receive more attention from researchers, but diseases have not yet seen extensive study. We do know that different growing environments, cultivation techniques, and strain or cultivar choices impact disease development. Of the many diseases associated with hemp, some of the more recent reports are presented. Among the foliar diseases, powdery mildew caused by

Golovinomyces spp. in BC, Canada, Kentucky, Ohio, and Oregon have all been reported on *Cannabis* (Punja 2018; Szarka et al. 2019; Farinas and Peduto Hand 2020; Wiseman et al. 2021). Powdery mildew caused by *Podosphaeria macularis* has been reported to occur in Oregon (Bates et al. 2021a) and in BC, Canada (Punja 2020b). Leaf spot symptoms derived from the casual agents *Bipolaris* spp. and *Cercospera* spp. as well as stem cankers due to southern blight caused by *Athelia rolfsii* have resulted in significant impacts to yield in Tennessee (Hansen et al. 2020). Other foliar diseases of importance include downy mildew, olive leaf spot, Sclerotinia stem canker, and other less commonly reported fungal, bacterial, viroid, and viral pathogens (McPartland 1996, 2003).

Soilborne diseases include root rots caused by *Fusarium oxysporum* (Punja 2020a; Thiessen et al. 2020), *F. solani*, *F. brachygibbosum* (Punja et al. 2018; Punja et al. 2019), and *F. graminearum* (Thiessen et al. 2020). Root rot of *Cannabis* has also reportedly occurred due to *Pythium dissotocum*, *P. myriotylum*, and *P. aphanidermatum* in Canada (Punja et al. 2019). Furthermore, there have also been reports of *Rhizoctonia solani*-infected crops in Tennessee (Hansen et al. 2020).

Pathogens of *Cannabis* floral organs include *Penicillium olsonii*, *P. copticola*, *F. solani*, *F. oxysporum,* (Punja et al. 2019), and *F. equisetii* (Punja et al. 2018). Of these *Fusarium* species, *F. solani* was noted to have caused the most severe bud rot symptoms (Punja et al. 2018). The powdery mildew species, *Golovinomyces cichoracearum* (Punja 2018) and *P. macularis* (Bates et al. 2021a), are also reported to infect the flowers of *Cannabis*. While only *G. cichoracearum* and *P. macularis* were reported to have been detected on flowers, it is plausible other powdery mildew species may infect *Cannabis* flowers. Additionally, *Sclerotinia sclerotiorum* was observed on hemp flowers in western Oregon during 2020 (C. M. Ocamb, personal communication). Of the pathogens known to impact the flowers of *Cannabis*, by far the most widespread and impactful floral disease is gray mold, incited by *Botrytis* species, primarily *B. cinerea* (McPartland 1996; Punja 2018, Thiessen et al 2020).

This list of pathogens contained above is not a comprehensive list of all pathogens known to impact hemp. While the list primarily focuses on those pathogens impacting *Cannabis* grown for CBD found in flowers, hemp grown for fiber and/or oilseed will experience different levels of disease severity, symptoms, and possibly range of pathogens. Greenhouse conditions which are often used for *Cannabis* production can also give rise to the presence of additional fungal diseases not commonly found under field conditions.

Botrytis

Botrytis is a fungus in the Sclerotiniaceae family and was one of the first genera of fungi described. This genus has since undergone reconstruction over the centuries since being first described in 1729, due to changes in genus concepts, age of the genus, and the relatively recent development of genomic tools used to designate fungal taxa. In 2020, there were 30 recognized species in the genus *Botrytis* that are collectively reported to impact more than 1400 cultivated crops (Elad et al. 2016). Comprehensive histories of *Botrytis* nomenclature and taxonomy are accounted for by Hennebert (1973), and more recently by Walker (2016). Among the *Botrytis* species, *B. cinerea* is recognized by some plant pathologists as one of the most important pathogens not only in this genus but among all pathogenic genera, owing primarily to its negative impact on pre- and post-harvest yields (Jarvis 1977) and recognition by the scientific community as an important pathogen for genomics research (Dean et al. 2012).

It wasn't until 2013 at the *Botrytis* Symposium in Bari, Italy that the *Botrytis* researcher community agreed upon the generic species name, *B. cinerea* (Elad et al. 2016). Prior to a single species name, plant taxa were given a teleomorph (sexual stage) name which was *Botryotinia fuckeliana* and an anamorphic name for the asexual stage, which is now its current name, *Botrytis cinerea*. Because of the vast host range of this fungus, *Botrytis* also has a broad geographic range, expanding from

temperate Alaska (Anderson 1924) to subtropical areas like Egypt (El-Helaly et al. 1962) and extending to every continent of the world (Jarvis 1977). With a pathogen capable of causing disease across the world on such a large number of crops and requiring pre- and post-harvest disease management, large economic losses are associated with this pathogen. While reliable estimates of crop loss are difficult to account for, reports suggest diseases caused by *Botrytis* spp. are responsible for up to $100 billion USD in annual losses worldwide (Boddy 2016).

Gray mold disease biology

Gray mold caused by *B. cinerea* has been investigated little on *Cannabis* because of the relatively short recent history as an agricultural commodity in the United States. While *B. cinerea* may be the predominant *Botrytis* spp. impacting flowers and stems of hemp, there are three *Botrytis* spp. known to cause gray mold in Oregon: *B. cinerea*, *B. pseudocinerea*, and an unnamed species (Garfinkel 2021). *Botrytis* is thought to be widely present in the landscape which may account for why aspects of reproduction, liberation, and dispersal of this pathogen lack sufficient research (Jarvis 1980).

Botrytis cinerea produces both primary inoculum and secondary inoculum. The overwintering or survival structures that function as a source of primary inoculum for *B. cinerea* include sclerotia, hyphae, and chlamydospores. Sclerotia may be the main source of primary inoculum for *B. cinerea* and sclerotia can persist for 5 to 9 months (Thomas et al. 1983), with survival ultimately determined by environmental factors such as its depth buried in the soil (Ellerbrock and Lorbeer 1977). Sclerotia can vary in size and are composed of mycelium encompassed in a melanized rind and an inner medulla containing a matrix of beta-glucans, both of which shield this overwintering structure from desiccation, ultraviolet radiation, microbial parasitism, etc. (Backhouse and Willets 1984, Pârvu and Pârvu 2014). Sclerotia of many *Botrytis* spp. go through carpogenic germination, giving rise to

apothecia bearing ascospores. Nonetheless, as noted by Carisse (2016), ascospores are considered a minor threat and in most cases, myceliogenic germination of sclerotia yields macroconidia, which then act as initial or primary inoculum. Microconidia can also arise from macroconidiophores or vegetation mycelium but are less common. Spore-bearing structures arising from sclerotia have been shown to sporulate for approximately 12 weeks under laboratory conditions (Nair and Nadtotchei 1987).

Although conidia are generally thought of as secondary inoculum and the source of secondary infections, they also play a major role in primary infections. Mycelium (a collective or mass of hyphae) is capable of overwintering in plant debris and seeds from the previous season. Overwintering mycelium lacks thorough investigation, making it difficult to determine how large of a role mycelium plays in overwintering of this fungus. Furthermore, *B. cinerea* is also known to produce chlamydospores, which can then result in either microconidia or macroconidia generation under both natural and artificial infections (Urbasch 1983; Urbasch 1986). It is thought that chlamydospores may offer an additional survival option during shorter, less favorable conditions (Urbasch 1983).

Secondary inoculum production by *B. cinerea* is largely crop specific and little has been investigated as to what temperatures, relative humidity levels, and time frameworks along with other factors facilitate conidial production on various plant species. Epton and Richmond (1980) suggested that formation of conidia is stimulated by specific wavelengths of light while Jarvis (1980) reported that conidiation by *B. cinerea* has an optimal temperature and wetness period that is dependent on the crop (Carisse 2016). Conidial release may occur due to several factors such as insects (Louis et al. 1996; Engelbrecht 2002), solar radiation, temperature (Blanco et al. 2006), leaf vibration, air movement, or water splash (Jarvis 1962a; Jarvis 1962b; Jarvis 1980; Carisse 2016). The primary dispersal of conidia is by wind and has three phases: liberation, transport, and deposition (Aylor 1990). Liberation is the freeing of conidia from the conidiophores, transport is the movement

of conidia from its origin to a new location, and deposition is the surface the conidia is deposited. The greatest level of conidia release is typically when the wind speed is fastest (Jarvis 1962b). Western Oregon tends to experience fastest wind speeds in early mornings and evenings absent of storm fronts. Periods with the fastest wind speeds are generally negatively associated with relative humidity and positively associated with increasing air temperature. The wind speed (Harrison and Lowe 1987), location in the canopy (Johnson and Powelson 1983), and conidial size are among the main factors influencing how far conidia can travel, and these should be kept in mind when considering disease management strategies. Conidia of *B. cinerea* reportedly traveled no more than a few meters in vineyards (Fitt et al. 1985) and snap bean fields (Johnson and Powelson 1983). The production of secondary inoculum is continuously created during the growing season, but the rate of reproduction appears to heavily depend on the crop (Carisse et al. 2015) and increases as the growing season progresses. The survival rates of conidia are affected by ambient temperature, moisture levels, microbial activity, and exposure to sunlight (Seyb 2003). In general, conidia of *Botrytis* spp. are thought to be short-lived (Holz et al. 2007). Upon deposition, *B. cinerea* conidia can form germ tubes within 1 to 3 hours in inoculation studies done under conducive conditions (Holz et al. 2007). Most investigations have been conducted *in vitro* and not much is known about *Botrytis* growth on a host surface or pathways used to enter and infect the host tissues (Holz et al. 2007; Carisse 2016).

Botrytis spp. can thrive under a range of environmental conditions, but environmental conditions along with several biological and agricultural factors will influence the development of disease. The two most important environmental factors for the germination of a *Botrytis* conidium are relative humidity and ambient temperature. While this pathogen is known for its extremely high genotypic and phenotypic plasticity, giving it the ability to adapt to many environments and allowing *Botrytis* spp. to persist within a broader spectrum of temperatures and humidity ranges, the optimal conditions are temperature generally between 15 to 20°C -with the presence of free water or a relative humidity above 93% (Carisse

2016). Generally, the minimum period of time during which the temperature and relative humidity requirements should be met is four hours, but the longer the conducive environmental conditions persist, the greater likelihood of an infection event, regardless of crop (Bulger et al. 1987; Broome et al. 1995). Cool to moderate temperatures and a high relative humidity are common conditions in the Willamette Valley of Oregon, particularly in the late summer and early fall, posing circumstances that are high risk to hemp plants for developing disease due to *Botrytis*. *Botrytis* is known to remain latent within the plant until the required environmental conditions are met in the infected host tissues. Once environmental conditions are favorable, it is only a matter of days before symptoms becomes visible, and shortly thereafter, disease can reach epidemic proportions if effective disease management strategies are not instituted (McPartland 1996).

Hemp floral organs serve as the primary infection court for *Botrytis* spp., but this fungus can also infect wounded tissues as well as senescing portions of a plant, and oftentimes will remain quiescent before symptoms develop. While the primary mode for *Botrytis* infection of hemp is not well studied, penetration is known to occur on other crop hosts through natural openings such as carpels (De Kock and Holz 1992) and stomata (Fourie and Holz 1995; Hsieh et al. 2001), although *Botrytis* may infect through an undamaged cuticle in some cases (Nelson 1951). Symptoms on hemp flowers begin with fan leaflets turning yellow and wilting followed by browning of the pistils. Soon after, flowers become covered in gray mycelium, conidiophores, and conidia, resulting in a gray to brown, fuzzy appearance that gives rise to the disease name, gray mold (McPartland 1996). Shortly after, disease can spread encompassing large portions to entire inflorescence (Figure 1.2). While gray mold on hemp flowers is a primary focus of this research project, *Botrytis* spp. also can cause damping-off of seedlings or incite stem cankers when plants are nearing full maturity, especially on cultivars grown for fiber production (McPartland 1996; McPartland et al. 2000).

Figure 1.2 Hemp inflorescence with single flower infected with *Botrytis*, the causal agent of gray mold (A); gray mold along an inflorescence after disease spread among flowers resulting in flower necrosis (B).

An improved epidemiological understanding of *B. cinerea* and other *Botrytis* spp. in hemp production along with the refinement of monitoring tools and sampling techniques is needed to accurately detect and quantify this pathogen. Despite improvements made by Carisse et al. (2009; 2015) in detection and quantification, there is still much that remains to be done, particularity for a relatively new crop like hemp. With an increased understanding of the epidemiology and improved ability to monitor *Botrytis* on hemp, IPM strategies can be developed that effectively and efficiently manage *Botrytis*-incited gray mold.

Management of gray mold

Management of *Botrytis*-incited gray mold is challenging but has seen large improvements in many crops over the past few decades, primarily due to the advent of fungicides effective for this pathogen. Where many crops have an array of available conventional fungicide active ingredients that can be applied individually or in unison to slow the spread of *Botrytis*-induced diseases, hemp has a very limited list of pesticide products registered for current use. As of December 2019, the EPA list of registered pesticides for use on hemp includes 56 biopesticides and one conventional pesticide (EPA, 2021). Currently, effective control of *Botrytis* on hemp primarily relies on cultural control methods, innate resistance of hemp lines, and biopesticides.

Cultural management practices

When crops are first introduced to a new region for cultivation, cultural control methods tend to be the first practices adopted for disease management. Cultural control modifies the plant environment in a way to reduce pest or pathogen pressure. Generally, these strategies are not only more economical to implement than chemical control methods, but also less detrimental to the local ecosystem. Cultural control of gray mold can be accomplished through varying means, but it is not always a one-size-fits-all approach and will work to varying degrees on individual farms.

One of the most successful methods to diminish the likelihood of a *Botrytis* epidemic is to decrease the relative humidity. *Botrytis* spp. are reliant on humid conditions for fungal growth and plant infection (Elad 2016). Greenhouses are commonly plagued with *Botrytis* outbreaks, and methods aimed at reducing the relative humidity are routinely utilized to aid in disease suppression (Nicot et al. 2016). Under field-based conditions, choosing sites with adequate wind movement that prevents air stagnation, increased spacing between plants and rows of plants, orientation of rows with the predominate wind direction, avoiding locations with higher relative humidity (especially late in the season), and reducing the presence of

free water on plants will help to decrease the risk for gray mold outbreaks (Elad 2016).

Other cultural controls such as removing dead and dying tissues, optimizing sanitation, exclusion, and avoidance methods can be employed to reduce the likelihood of *Botrytis*-incited gray mold being present in a production site. Because this pathogen is a necrotroph, removal of dead plant tissue prevents *Botrytis* from obtaining the foothold it oftentimes requires for disease. This ties in closely with maintaining a strict level of sanitation in hemp production. Plant debris, trimmings, etc., should ideally be removed from production fields and greenhouses. By doing so, potential infection courts and inoculum sources are removed, reducing the threat from *Botrytis*. Exclusion of the pathogen can be accomplished by growing indoors, using greenhouses with filtered air circulation to prevent *Botrytis* introduction, cultivation in regions where *Botrytis* is not as well established, or using faster maturing hemp cultivars to avoid late season rains and subsequent disease development.

Biopesticides and biological control practices

Biological control agents and biopesticide formulations targeting *Botrytis* on a number of crops have shown limited success despite extensive research efforts (Nicot et al. 2016). As previously noted, outbreaks of *Botrytis* on many crops have been primarily managed via the applications of synthetic fungicides with various modes of action (Leroux 2007; Balthazar et al. 2020). Currently, biopesticides for targeting *Botrytis* on hemp lack sufficient evidence to recommend for their use to control this pathogen. Because hemp has had restrictions or bans on production until just recently, very little research has been conducted into the management of *Botrytis* by biological control means, let alone conventional fungicides. Furthermore, the stringent laws surrounding chemical residue levels on hemp products as well as chemical company concerns about product usage in marijuana (recreational *Cannabis* grown for THC), all extend the difficulty of developing effective fungicide spray programs for controlling key diseases in hemp production (Seltenrich 2019).

More recently, attempts have been made at understanding biological control agents and bear promising results (Lyu et al. 2019; Balthazar et al. 2020; Taghinasab and Jabaji 2020). These studies attempt to address biological control and the potential development of biopesticides by decoding the phytomicrobiome of hemp. There is optimism for discovery of closely associated microorganisms that may potentially serve as biocontrol control agents for plant pathogens (Lyu et al. 2019). Significant breakthroughs in this current pursuit of research and development haven't been seen as of yet, but the envelope of biocontrol used to manage *Botrytis* on hemp has been pushed forward and has not been entirely unsuccessful. Use of a biopesticide on hemp has been shown to decrease *Botrytis* incidence and severity in a recent field trial in the Willamette Valley of Oregon (Bates et al. 2021b). Despite the dearth of research suggesting biocontrol methods are capable of preventing *Botrytis* epidemics, a growing list of EPA-registered biopesticides and the current biopesticides in other cropping systems is signaling success (Abbey et al. 2019), supplying some confidence for the use and future development of biological control methods.

Hemp genetic lines

Hemp breeding can lower gray mold risk in numerous ways. One approach is generating hemp cultivars that avoid disease via early maturation. Hemp cultivars can be divided into two groups, photosensitive and auto-flowering lines. Daylight sensitive or photosensitive hemp cultivars transition from vegetation growth to flowering based on the number of hours of light exposure. From the time flowering begins, hemp flowers generally take 7 to 10 weeks to fully mature and are then ready for harvest. Cultivars that have a lesser flowering time length or begin to flower sooner avoid late season conditions of higher humidity, cooler temperatures, shorter day lengths, etc., all of which can increase gray mold disease pressure. Moreover, hemp cultivars referred to as autoflowering do not transition from vegetation growth to flowering based on photosensitivity, but rather have an 8- to 11-week period to maturation from seed to harvest. Autoflowering hemp is developed through breeding a combination of either *C. sativa* or *C. indica* with *C. ruderalis*, which is native to

central and eastern Europe, but the origins of autoflowering hemp are not fully understood (Punja et al. 2017). These *C. ruderalis* crosses are able to survive during shorter growing seasons. The shortened time from sowing to full maturity allows for hemp harvest prior to the onset of environmental preferences conducive for *Botrytis,* resulting in exclusion of the pathogen. While *Botrytis* is still capable of causing flower rot post-harvest on *C. ruderalis* crosses, this disease aspect can be managed through proper storage conditions.

Finally, plant structure can play an important role in *Botrytis* suppression. Larger, more dense hemp flowers tend to exhibit the greatest incidence and severity of gray mold. This is most likely the result of trapped moisture and/or a higher relative humidity within the flower parts, resulting in favorable conditions for *Botrytis* infection (McPartland 1996). Hemp buds that are smaller and less compact are generally considered unfavorably by hemp growers harvesting flowers, but the smaller buds would be preferable for disease suppression. Finding a balance of flower size and compactness with yield may prevent gray mold via plant characteristics. Additionally, hemp cultivars with plant structure conducive for maximizing airflow will help to reduce periods of free water and high relative humidity. Plants that aren't as dense, nor as compact, or shorter in stature would allow for more sunlight and increased airflow to penetrate the plant canopy.

Remote sensing

Unmanned aerial vehicles (UAVs) are a new tool being adopted by growers to scout fields via remote sensing to assess plant health and disease levels in agricultural fields. Remote sensing is the nondestructive observation of an object(s) or phenomenon (Lillesand et al. 2015). This is typically accomplished with an optical sensor that collects data at a specific wavelength or a range of wavelengths (spectral bands) within the electromagnetic spectrum. One of the first applications of remote sensing was made in the early 1900s using panchromatic filming of aerial flights

during World War I (Moore 1979). Remote sensing with optical sensors was not applied in agriculture until the mid-1900's, where black and white aerial photography was conducted by the U.S. Department of Agriculture. Upon recognition of the billions of dollars lost to pests and diseases, the Agricultural Board of the National Research Council created the Committee on Remote Sensing for Agricultural Purposes in 1961 to help gain insights on management strategies (Macdonald 1984). It was not until 1970 that a researcher attempted to collect information in a plant pathology context for an agricultural system when Pisharoty used remote sensing in a manned aircraft flown at 500 and 1000 feet above ground level for detection of coconut root wilt disease (Dakshinamurti et al. 1971).

The inception of remote sensing and its subsequent progression were driven by potential applications for the U.S. military. With the spark of the digital revolution and technology advancements booming, newer optical sensors and aircrafts were developed at a rapid pace in the 1960's. More importantly, optical sensors were being designed specifically for agricultural applications. Presently, more powerful camera options have become available and more affordable. Additionally, we are no longer limited to using satellites or airplanes to collect imagery, as we now have access to small fixed-wing and multicopter UAVs. These newer flight platforms have many advantages over previous systems used for aerial data collection, especially for plant disease detection. The combination of recently developed sensors and UAVs, along with sophisticated machine learning models, has opened a door to many possibilities in the application of precision agriculture.

Optical sensors used in remote sensing

There are a relatively small number of sensors currently undergoing evaluations for their ability to gather information on crop health. Researchers and other workers within the precision agriculture industry are seeking to find the optimal sensor types and spectral band requirements needed to approximate crop yields,

nutrient deficiencies, pests, pathogens, phenotypes, and more via remote sensing. No single sensor will offer the best solution to the broad range of plant-related issues. Some of the more common optical sensors include chlorophyl fluorescent, thermal, LiDAR, visual spectrum (RGB), hyperspectral, and multispectral (Araus and Cairns 2014; Mutka and Bart 2015; Sankaran et al. 2015; Mahlein 2016; Zhang et al. 2019).

The most success for disease detection has come through the application of hyperspectral and multispectral sensors (Sankaran et al. 2015; Zhang et al. 2019). The distinction between the two is arbitrary; multispectral is simply an optical sensor which collects information at nine or fewer spectral bands where hyperspectral is ten or more (Lamb 2000). Typically, this includes bands in the visible spectrum of light, referred to as RGB, which includes the red, green, and blue wavelengths. More capable sensors extend into the far-red and near-infrared regions of the electromagnetic spectrum and are commonly used for disease detection (Sankaran et al. 2010; Abdulridha et al. 2019; Lu et al. 2018; Dammer et al. 2011). Both multispectral and hyperspectral sensors have positive and negative attributes associated with their use, but their implementation ultimately comes down to the goals of the user.

Band lengths for multispectral optical sensors tend to range from 10 nm to 50 nm but are generally broader in the infrared regions (Deng et al. 2018). As with many of the remote sensing tools, sensors are developed to satisfy a specific purpose which directs the number, size, and placement of the spectral bands. Larger spectral bands have a lack of spectral resolution making it difficult to discern subtle differences in the electromagnetic spectrum observed between features. The primary advantage of hyperspectral cameras over multispectral is their ability to resolve features in the electromagnetic spectrum because of their increased spectral resolution. Finding differences in spectral bands is a key requirement for plant disease detection. The use of spectral indices or vegetation indices has become a primary approach for disease detection by multispectral users due to the lower spectral resolution (Yang et al. 2007; Naidu et al. 2009; Behmann et al. 2014; Candiago et al. 2015). A vegetation index is

a spectral calculation between bands meant to reveal characteristics of the plant not apparent otherwise. Many vegetation indices have been developed over the past few decades, including spectral indices designed for a single disease (Mahlein et al. 2013). Camera selection should consider both narrowband and broadband sensors as well as which bands allow for spectral index calculations required for detection of a particular disease (Deng et al. 2018).

Two additional resolutions important to plant disease detection include the radiometric and spatial resolution. Cameras have different radiometric resolutions which are reflected in the number of 'bits' the camera has. A 12-bit camera for example will have a possible 2^{12} range of digital numbers per pixel based on the spectral reflectance. A high digital number will be representative of high reflectance at a given spectral band, while a low digital number indicates low reflectance. In essence, a higher radiometric resolution will provide greater detail of the spectral characteristics of measured features. Similarly, higher spatial resolution results in a finer detailed image through increasingly smaller-sized pixels. The coupling of high spatial and radiometric resolution gives the user better quality images.

Sensor weight, cost, and data storage are three other components worth considering when selecting a camera for disease detection techniques. Multispectral cameras strike a balance between cost and weight (Deng et al. 2018). With the adaptation of drones for aerial imaging, compact and light weight cameras are needed to maximize flight time of the UAV. The optical sensors fixed to the drone can have one of greatest influences on duration of flight time. Sensors designed for UAVs will have as much weight shaved off as possible but that may come at a cost. High quality multispectral sensors can be currently purchased for $10,000 USD or less whereas hyperspectral sensors are five times or more expensive and generally weigh more. Finally, the amount of data collected by a hyperspectral camera can be burdensome for storage and processing. Hyperspectral sensors will require vast storage space within the UAV during flights and a powerful computer for processing data.

Aerial platforms used in remote sensing

The platform by which an optical sensor is mobilized is integral for quality data collection required for plant disease detection goals. The primary aerial platforms used for disease detection by remote sensing include satellites, manned aircrafts, and more recently, UAVs. While all these platforms have shown to be successful in disease detection, UAVs are better adapted for the specific needs of disease detection (Garcia-Ruiz et al. 2013). Satellites have variable temporal resolutions, but in comparison to both manned and unmanned aircrafts, satellites have the lowest temporal resolution. Additionally, data derived from satellites are going to have the lowest spatial resolution, followed by manned aircrafts, and the greatest spatial resolution come with UAVs. Unmanned aerial vehicles are also lower in cost in comparison to manned aircrafts (Wing et al. 2014) and the availability of UAVs, such as fixed wings and multicopters, has increased accessibility for a larger community of users (Araus and Cairns 2014).

The temporal resolution of an aerial platform is important for meeting disease detection goals. Experienced growers, agronomists, and researchers have a strong sense of when disease is likely to show up in a field. This may be after heavy rainfall, periods of minimum or maximum temperatures, the time of the season, growing degree-day models, or visual disease observations that drive these approximations. Researchers and managers should align aerial surveys with anticipated disease detection windows or immediately after visual observation. Satellites have a fixed schedule based on their orbit and are therefore, limited in their ability to collect data on a moment's notice. Manned aircrafts typically require a hired pilot which can be more costly and may not actually be available for flights when it is necessary. Unmanned aerial vehicles, commonly referred to as drones, allow for flexible flight schedules not easily accomplished with manned aircrafts or satellites (Deng et al. 2018). The issues of temporal frequency and spatial resolution are addressed by the adaptation of UAVs in data collection (Lelong et al. 2008). While issues such as cloud cover, rainfall, high winds, or other environmental conditions may result in

UAV limitations, it still stands as the best option for meeting the necessary flight times for data collection.

As mentioned previously, spatial resolution is a critical limiting factor for disease detection by remote sensing. In order to capture the signs or symptoms of a disease, high spatial resolution is pertinent. While satellite spatial resolution continues to improve, their lack of high spatial resolution is still one of the greatest drawbacks for remote detection of plant diseases using satellites. High spatial resolution satellite imagery used in measuring plant characteristics is scaled in meters (Li et al. 2019) as compared with centimeters or millimeters through in UAVs. Because plant disease symptoms or signs cannot be observed with such low spatial resolution, obvious challenges arise. Manned aircrafts can fly at lower distances to the ground but not as low or controlled as UAVs. While both satellites and manned aircrafts are capable of much greater payloads than UAVs, resulting in more powerful optical sensors, this does not generally offset their increased spatial distances from the object being measured. Unmanned aerial vehicles can ultimately fly as low as disease detection surveys necessitate. Issues such as chopper spray, danger of hitting the plant canopy, and hazards such as surrounding trees or telephone wires are a concern but can be managed with careful flight planning. The lower flight altitudes permitted by UAVs allow for the highest spatial resolution, down to millimeters in size, providing the resolve needed for detecting plant disease.

Unmanned aerial vehicles can be divided into four groups: parachutes, blimps, rotocopters, and fixed-wing aircrafts (Sankaran et al. 2015). More recently, the development of hybrid platforms, a combination of fixed-wing and multirotor UAVs, have increased in popularity. For disease detection and most agricultural uses in general, rotocopters and fixed-wing aircrafts have outcompeted the other models in development and are now a staple of aerial detection platforms in agriculture. A fixed-wing aircraft is an airplane that uses the wings to generate lift whereas a multicopter uses the rotary speed of its many rotors to generate lift. Fixed-wing aircrafts have the advantage of longer flight times and increased speeds leading to

greater range in comparison to multicopters (Sankaran et al. 2015). Alternatively, multi-rotor UAVs are able to hover and are more easily flown at lower elevations and with greater precision. Both rotocopters and fixed-wing aircrafts offer advantages and disadvantages worth considering and choices should be based on needs of the researcher or growers' goals.

Precision agriculture and UAVs

Precision agriculture can be defined as "a management strategy that uses information technology to bring data from multiple sources to bear on decisions associated with crop production" (Candiago et al. 2015). The crossroads between agriculture and geographic information science (GIS) essentially gave rise to the precision agriculture concept and practices of the early 1980's. Application of this new farming strategy was not routinely applied until 1988 with the SoilTeq (Fairchild 1988), a fertilizer blender and distributer (Stafford 2000). Much of the applicability of precision agriculture came with the advent of the global positioning system (GPS). But early on, the GPS was a challenge for the lay person to adopt into practice, and further efforts to increase its reliability and usability were needed (Stafford 2000). By the early 1990s, maturation of the GPS and other technologies led to a rapid expansion in adoption for agriculture and inspired the development of spatially variable herbicide applicators (Stafford and Miller 1993), soil organic matter sensors (Price and Hummel 1994), yield mapping technology (Pierce et al. 1997), and more. The early adoption of precision agriculture is highlighted in studies by Daberkow and McBride (2000; 2003), and Griffin and DeBoer (2005). Within a few decades of development, the objectives of precision agriculture to optimize available resources for increased profits, decrease negative environmental impacts, and improve the workplace environment and social aspects of agriculture have been used to help address farming problems across the world (Gebbers and Adamchuk 2010).

Some of the more popular precision agriculture tools are auto-steer systems, variable rate technology for input applications such as fertilizers, and GPS-based mapping systems for crop health (Schimmelpfennig 2016), dating back to the late 1990's (Lambert et al. 2004). Others include yield, field, soil, and crop sensors, robotic harvesting systems, and remote sensing (Zhang et al. 2002). Trimble Agriculture suggests aerial imaging through satellites and UAVs will be one of the primary tools used in crop management in 2021 (Trimble Ag. 2021). Places like Canada, Europe, Asia, and South America tend to incorporate UAVs in agricultural practices more often than the U.S. due to the lack of airspace and licensing restrictions (Stehr 2015). Despite a relatively slow start for remote sensing, largely because of the low spatial resolution of satellite and manned aircraft data (Zhang et al. 2002), the Association for Unmanned Vehicle Systems International is expecting an 80 to 90% growth in the UAV market coming from agricultural use (Karst 2013). Drones are expected to be popular for use in mid-season crop health monitoring, irrigation equipment monitoring, weed identification, variable-rate fertility (Veroustraete 2015), water monitoring, nutrient monitoring, identification of disease stress, and much more (Daponte et al. 2019). The opportunities to incorporate precision agriculture are not limited to crop production but have value pre- and post-harvest as well. Precision agriculture is a very broad concept that encompasses more than just the technologies but also the generated data. Making use of big data has been a major roadblock for precision agriculture users (Erickson and DeBoer 2020). Applying data derived from precision tools correctly takes practice or a trained expert and is critical to receiving farm profits. In the early 2000's, it was difficult to understand the financial benefits of adopting precision agriculture approaches (Lambert et al. 2004). Recent economic studies looking at adoption of precision agriculture by Erickson and DeBoer (2020), Schimmelpfennig (2016), and Griffin et al. (2018) have brought to light which types of agricultural producers this technology can help and how farmers can benefit from adopting precision agricultural approaches.

The tools of precision agriculture were initially utilized by larger farms, and adoption over the years has mostly been limited to these larger producers. In the early 2000's, utilization of precision agriculture technologies was up to 22% of U.S. growers cultivating the dominant row crops such as corn and soybean (Schimmelfennig 2016). A 2010 USDA Agricultural Resource Management Survey (ARMS) provides data showing that corn and soybean farmers are more prone to the adoption of precision agriculture tools where yield monitoring is used by about half of these farmers, representing about 70% of U.S. dent corn and soybean acreage (USDA ARMS 2010). The disproportion of acreage versus the percentage of farmers utilizing precision agriculture suggests that smaller farms are less likely to adopt these tools compared to larger farms. In this same 2010 study, 12% of corn farms with less than 600 acres used yield mapping, guidance systems, and variable rate technology. Alternatively, corn farms greater than 3,800 acres used precision agriculture technologies at a much greater percentage; yield mapping was used on 80% of these corn farms, 84% used a guidance system, and 40% used variable rate technology. Schimmelfennig (2016) suggests implementation of these technologies on farms was largely driven by not only farm size, but also by machinery used and farm labor costs. Location also seems to influence where these tools are most often used. Because many of these major crops are grown in the middle of the U.S., it is not unexpected that precision agriculture technology is used more often in the Midwestern U.S. (Erickson and DeBoer 2020) and the corn belt region of the U.S. (Schimmelfennig 2016). But the trend of precision agriculture adoption for cultivation practices by farmers has certainly gone up from its inception in the 1980s till now. Agronomy companies across North America have launched precision agronomy programs. At most agronomy companies, you can now find an employee with the job title, 'Precision Agronomist'. In a survey offered to mostly agricultural retail input suppliers, they were asked whether or not they would be offering nine service- and sensor-related precision agriculture technologies over the next three years, and all technologies saw an upward trend in offerings (Erickson and DeBoer 2020). Universities, such as South Dakota State, are recognizing these trends toward a new

age in agriculture and have created a degree in precision agriculture. While precision agriculture is gaining traction as an emerging farm practice, some precision agriculture tools have seen more development and usage than others because of the financial benefits gained.

While the effect of precision technologies on corn farms, based on USDA economic research service data, has a positive net return of 1.1 to 1.8% compared to those who don't use them, precision technologies are not a one-size-fits-all (Schimmelfennig 2016). Many variables come into play which impact the net returns seen with utilization of precision agriculture tools. In compensation for the fact that precision agriculture efforts have primarily targeted the major row crop systems in the U.S., a large amount of funding in the past decade has gone towards research and development of precision agriculture utilization for specialty cropping systems, which composes about one-third of U.S. agricultural crop receipts. Between 2008 and 2018, the USDA funded $287.7 million USD on the increased development and utilization of automation in the production and processing of specialty crops. Between 2010 and 2018, another $3.4 billion USD was granted for the development of digital infrastructure for increased automation and mechanization as well (Astill et al. 2020). Universities funded by federal grant programs have pushed to move conventional agriculture practices toward precision agriculture. This effort has not been futile, and adoption of these tools by the industry are increasing. On a survey with over 20 precision technology service offerings, dealerships showed anywhere from 71% of the retailers making a profit on variable-rate technology fertilizer application down to 0% on robotic crop scouting or weeding, but with 85% responding they were unsure about profits on the latter (Erickson and DeBoer 2020). The global precision agriculture market was valued at $4.7 billion USD in 2019 and is estimated to increase at a compound annual growth rate of 13.0% from 2020 to 2027 (Grand View Research 2020). Drones are expected to play a major factor in future farming trends and are listed at $9.9 billion USD in 2019 and expected to grow at 7.1% from 2020 to 2025 (Mordor Intelligence 2020). Precision technology is the future of agriculture and is now being recognized as such by those in the agricultural industries.

Remote sensing of plant diseases

Most of the literature emphasizes the utilization of multispectral or hyperspectral digital images for disease detection (Barbedo 2013), but in the infancy of disease detection by remote sensing, RGB was the most commonly used method and still has value because of its low cost and ease of use. Many studies have reported success using RGB images for disease detection (Camargo and Smith 2009a; Camargo and Smith 2009b; Arivazhagan et al. 2013; Neumann et al. 2014; Barbedo et al. 2016). Reviews by Barbedo (2013; 2016) give practical explanations for why RGB is still relevant for disease detection. Despite RGB's ability to detect plant diseases, studies that have compared RGB and multispectral images most often report that multispectral cameras are more proficient for disease detection (Dammer et al. 2011; Abdulridha et al. 2019). Much of this is likely attributed to the reflectance of vegetation in the near-infrared region of the electromagnetic spectrum often captured in multispectral data but not RGB.

A large portion of reports on disease detection via remote sensing utilized controlled environments for experiments. This ignores the reality of field-like conditions where plants are often exposed to many pathogens or pests and are influenced by abiotic factors such as nutrient deficiencies or drought stress. Predictive models generated on healthy plants void of any abiotic symptoms or other pathogens, generally lack the ability to accurately predict disease when put into field-based applications. A limited number of studies have had success using predictive disease detection through remote sensing on plants with two or more pathogens (Franke and Menz 2007; Mahlein et al. 2010; Rumpf et al. 2010). Additionally, detection of abiotic factors by remote sensing, such as leaf nitrogen content (Cohen et al. 2010; Vigneau et al. 2011), drought stress (Winterhalter et al. 2011), and a range of soil properties (Rossel et al. 2006) have also been successful. But many of the studies fail to simultaneously detect disease in the presence of abiotic and biotic factors (Abdulridha et al. 2019, Ferentinos et al. 2019). The easiest way to accomplish this is by field-based data collection rather than using greenhouse- or lab-grown plants.

Early stages of model optimization may focus on accurate prediction of abiotic or biotic factors influencing plant health *ex situ*. But future work should be extended to *in situ*, where many practical aspects of disease detection by remote sensing can be utilized. Detailed reviews on digital image classification of plant diseases have been conducted and include a range of host-pathogen systems which have had successful disease detection model creation, and where the future research should focus to increase scientific breakthroughs (Sankaran et al. 2015; Mahlein 2016; Thomas et al. 2018). While remote sensing is not an instant solution to the complex task of plant disease identification and quantification, it is proving to be a very useful tool for researchers, agronomists, and agricultural producers.

Remote sensing of black leg on turnip and gray mold on hemp

This thesis covering case studies on remote sensing and machine learning used for disease detection of black leg on turnip and gray mold on hemp addressed two research questions. Firstly, can remote sensing and machine learning be used to detect the diseases black leg on turnip and gray mold on hemp? Secondly, can the combination of remote sensing and machine learning be used as an alternative disease detection method for traditional field-based techniques?

Disease detection through traditional techniques such as field scouting on foot, molecular assay methods, or morphological identification of plant pathogens is time consuming and costly. While molecular testing techniques may be more objective than visual identification of disease, it generally does not provide insights on disease incidence or severity levels and requires an unpredictable length of time to accomplish and resources unavailable to the grower (Barbedo 2016). Additionally, collecting samples from the field as well as field scouting on foot can be destructive to crop plants.

Under these circumstances, it seems sensible to investigate alternative methods that mitigate these shortcomings or concerns with traditional field sampling

techniques for disease identification. Digital image collection by UAVs, coupled with machine learning, is a newer method with a record of success (Mahlein 2016). Machine learning can be defined as the study of artificial intelligence used in computer algorithms that learn from data and improve accuracy automatically through experience. Remote sensing combined with machine learning for disease detection provides a more objective method of field sampling that can be nondestructive, inexpensive, and potentially faster than traditional techniques.

Considering that plant diseases can have devastating impacts on crop yields if not addressed appropriately, the research described in this thesis provides a case study on digital image analysis with machine learning techniques for detection of two different diseases important in western Oregon crop production, black leg on turnip grown for seed and gray mold on hemp. The contrast between the utility of remote sensing for disease detection in these two different disease systems are covered in detail. The applicability for disease incidence assessment is presented. A detailed methodology for application of disease detection under field conditions in hemp and *in situ* for turnip is conducted and the viability for agronomists, growers and researchers is discussed.

Chapter 2: Materials and Methods

Model building and application of plant disease detection via remote sensing and machine learning can be broken down into five steps: data acquisition, data processing, model training, model testing, and application. The first case study is on the detection of black leg on turnip and methods are assessed in this framework. This is followed by the second case study, gray mold one hemp, which utilizes these similar steps and addresses application in a biofungicide field trial.

2.1 Turnip sites

Turnip leaves affected by black leg were collected on 7 and 15 March 2019 from two commercial farms in the Willamette Valley. Unmanned aerial vehicle (UAV) flights were also conducted at these fields on the same dates and were selected based on cloud-free days during the winter months when leaf spot could be observed (Figure 2.1). Symptomatic leaves were sufficient in supplying enough plant material representative of healthy tissue and diseased, and were the only leaf samples collected. *Leptosphaeria* spp. causing black leg leaf spots in selected turnip seed fields were not confirmed with molecular testing or microscopic morphology but were documented with images and determined to be *Leptosphaeria*-induced leaf spots based on characteristic symptoms and signs. Following UAV flights and the collection of 100+ diseased leaves from each location; leaves were taken to the lab and either placed in the cold room (~5°C) for preservation at a maximum of 48 hours or immediately used for image collection.

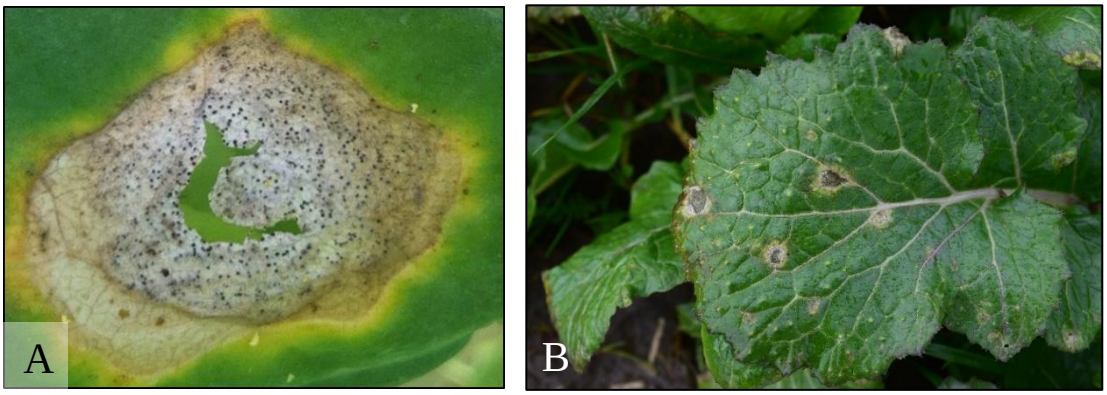

Figure 2.1 Leaf spot on turnip leaf showing pycnidia and shothole effect of fragile plant tissue, typical of a leaf spot caused by *L. maculans* and/or *L. biglobosa* in western Oregon (A). Turnip leaf displaying symptoms of leaf spots characteristic of black leg (B) (Image A by C. M. Ocamb).

2.2 Turnip data acquisition

A Micasense RedEdge - M (AgEagle Aerial Systems Inc., Seattle, Washington) (Table 2.1) optical sensor containing five multispectral bands was fixed to a UAV platform, the DJI Matrice 210 RTK (SZ DJI Technology Co. Ltd., Shenzhen, China) (Table 2.2). The UAV was flown at 10 m and 20 m above ground level on 4046 m^2 between 11:00 a.m. and 1:00 p.m. Flights contained 80% image overlap and a double grid flight pattern using the DJI Pilot software (SZ DJI Technology Co. Ltd., Shenzhen, China). A reflectance panel was imaged before and after flights for radiometric calibration.

The Micasense RedEdge – M optical sensor was also mounted to a PVC structure approximately 1.5 m above ground level with a power cable running to a laptop serving as the power source. The optical sensor was directed downward where the sensor view area included a black tarp and plastic tray as the background with a single turnip leaf placed at the center. Beside the tray was a reflectance panel used in radiometric calibration (Figure 2.2). Turnip leaves with leaf spots characteristic for black leg were imaged outdoors under the PVC structure between 11:00 a.m. and 1:00 p.m. to ensure properly lit photos. Images of 60 to 100 turnip leaves were

collected for each of the two field locations on both dates with a spatial resolution of ~0.1 cm and with a radiometric resolution of 12 - bit.

Table 2.1 Spectral bands and associated bandwidth of the Micasense Rededge - M optical sensor used to collect image data of turnip leaves growing in fields affected by black leg

Band name	**Bandwidth (nm)**
Blue	465 - 485
Green	550 - 670
Red	663 - 673
Near Infrared (NIR)	820 - 860
Red edge	712 - 722

Table 2.2 Specifications of the DJI Matrice 210 RTK drone used in remote sensing survey of a hemp research field on the Oregon State University Botany and Plant Pathology Field Laboratory

UAS Model	M210 RTK
Dimensions unfolded	887 × 880 × 408 mm
Weight (with two TB50 batteries)	~ 4.42 kg
Maximum payload weight (with TB50 batteries)	~ 1.72 kg
Maximum flight time (no payload, with TB50)	23 min

Figure 2.2 The red band image of PVC structure, calibration panel, background tarp, black plastic tray, and a single plant leaf enclosed by the identifying red circle. Leaf spots are apparent on the leaf, appearing as gray to whitish-colored areas.

2.3 Turnip data processing

Flight data was determined to have insufficient spatial resolution at 10 m above ground level. This was determined by assessing individual images in ArcGIS Pro version 2.2 (ESRI, Redlands, California) by zooming in to view individual turnip leaves on the turnip plant, leaf spots could not be seen in any of the five spectral bands. Flights below 10 m resulted in too much chopper spray that disturbed the plants with wind movement, and required manual flights rather than autonomous ones. So, the remainder of the black leg on turnip case study utilized images taken at 1.5 m from the PVC structure. These images were uploaded into ArcGIS Pro for image processing. No radiometric calibration was applied to the image set. Five to ten images of turnip leaves were selected from each location on each date based on visual appearance of symptoms seen in the red band, and all five bands of each turnip image

were uploaded into ArcGIS Pro. Because the lens for each optical sensor associated with the five bands are located in a different position on the camera, a slight difference in the field of view for each band resulted in images with improper overlap. To correct this, georeferencing options in ArcGIS Pro allowed for movement of the near infrared (NIR) band 8 pixels down to get a proper overlap of the of the NIR and red band image scenes. All images were adjusted, and the NIR band and red band were used to create the normalized difference vegetation index (NDVI) for each of the turnip leaf images (Table 2.3).

2.4 Turnip model training and testing

Training data were then generated in ArcGIS Pro by manually selecting black leg-affected pixels and pixels representing healthy tissue from 10 of the turnip images, and utilizing at least one turnip leaf from each of the two fields on each date. These images were selected because they contained characteristic leaf spots caused by black leg. Training data derived from the red band and NDVI were uploaded into RStudio Version 1.3.1093 (R, Boston, Massachusetts) and used for training the support vector machine (SVM) model (Hearst et al. 1998; Kuhn 2020; Meyer et al. 2020) and subsequent validation testing. SVM uses a hyperplane to separate and classify data points by minimizing the distance between data points and the line using support vectors, hence the name, support vector machine. A hyperplane is a decision boundary and points that fall on one side or the other, and are attributed to separate classes. Support vectors are only data points within a margin of the hyperplane and define the model hyperplane. The digital numbers, commonly referred to as the pixel value, of the training data derived from the 10 images were merged and partitioned into 70% for training and 30% for testing. A SVM model was used and trained with 1576 pixels, with approximately equal black leg-affected pixels and healthy leaf tissue pixels. The accuracy of the model was assessed with 676 pixels in the testing data set and used to create a confusion matrix for model assessment looking at accuracy, specificity, sensitivity, false positives, and false negatives. Cohen’s Kappa

coefficient is another assessment of model accuracy which grants a metric of agreement between user-defined classes and assigned classes by the predictive model, and also considers accuracy generated by random chance (Cohen 1960). This ranges from -1 to 1, where 1 indicates complete agreement between the user and classifier. Cohen's Kappa was once regarded as more robust than overall accuracy and the best assessment of machine learning accuracy, but has recently seen criticism due to its redundance to accuracy and therefore, should not be used alone for model assessment (Pontius and Millones 2011; Olofsson et al. 2014). Model assessment for our research purpose is primarily focused on the balance of accuracy, sensitivity, and specificity, and included Cohen's Kappa for those who still value its model assessment capabilities. Sensitivity is the proportion of the pixels predicted as positives that were positives (true positives). Specificity is the proportion of classified negatives by the model that are negatives (true negatives). This model was applied to all the pixels of four turnip leaves extracted from the black background to visually assess accuracy and provide practical application to this process.

2.5 Hemp site

On 18 June 2020, 0.28 hectares (2833 m^2) of the hemp cultivar 'White CBG' were planted at the Oregon State University Botany Field Laboratory in Corvallis, Oregon for a biofungicide efficacy trial for gray mold on hemp (Figures 2.3 and 2.4). This field study utilized a randomized block design containing five replicate-blocks with four treatments, including a nontreated control. Each plot consisted of two rows of 10 plants spaced at 1.8 m between rows and 1.2 m between plants within rows. Two plant buffers of untreated hemp were used between replicate blocks and three plant buffers between plots within each block provided a 3.7 m spray buffer. A broadcast fertilizer of Nutri Rich (Stutzman, Canby, Oregon) 4-3-2 with 7% Ca at 544 kg/A was applied one week prior to planting and again at 54 kg/A the first week of bloom, which began 13 July ± 4 days. Weeds were mechanically controlled by

hand and overhead irrigation was applied when necessary. Details of this study can be found in Bates et al. (2021b).

Figure 2.3 An aerial perspective of the hemp field study site on the Oregon State University Botany and Plant Pathology Field Laboratory taken at 10 m above ground level on 7 Oct 2020.

Figure 2.4 The hemp research plot on 9 Oct 2020 at Oregon State University Botany and Plant Pathology Field Laboratory (A). Hemp flowers exhibiting gray mold, induced by *Botrytis* species (B). A hemp plant with severe gray mold on multiple inflorescence (C).

2.6 Hemp data acquisition

Field level survey

From June to October, *Botrytis* spp., *P. macularis*, and *Fusarium* spp. were observed causing disease within the hemp field, with the first visual observation of *Botrytis* occurring on 22 September 2020. Visual assessments of disease incidence in the uppermost 30-cm portion of eight individual inflorescence on each of five randomly chosen plants in each plot were made on 25 Sep, 2 Oct, and 9 Oct 2020. Incidence data were analyzed as repeated measures in a generalized linear mixed model assuming a binomial distribution of the response variable. Treatment, rating date, and their interaction were fixed effects. Replicate block was a random effect. Temporal correlation of residuals was modeled assuming a first-order autoregressive covariance structure. Analyses were conducted using the GLIMMIX procedure in SAS version 9.4 (SAS Institute, Cary, North Carolina).

Aerial survey of field

UAV flights were conducted on 26 Aug, 22 Sep, and 7 Oct 2020 between 11 a.m. and 1 p.m. for each flight. The UAV was flown at 10 m above ground level and ranged from a 21 to 24 min in duration with 80% image overlap and a double grid flight pattern covering 3642 m^2 using DJI Pilot software. A reflectance panel was imaged before and after flights for radiometric calibration. The aircraft platform was the DJI Matrice 210 RTK (Table 2.2) with a Micasense RedEdge - M (Table 2.1) optical sensor containing five multispectral bands. Spatial resolution was 0.69 cm with a radiometric resolution of 12-bit.

2.7 Hemp data processing

Images were uploaded and processed by Pix4Dmapper version 4.5 (Pix4D, Prilly, Switzerland) to generate an orthomosaic for each band in addition to a digital elevation model. This software automatically detects images containing the

reflectance panel and applies a radiometric calibration across the image set. A PDF document from Pix4D provided flight statistics and was used to ensure flight images were accurately geotagged, overlapped, and radiometrically calibrated. Raster-based images derived from Pix4Dmapper were then uploaded to ArcGIS Pro for vegetation indices calculation and raster development. The band combinations and names used for vegetation index creation are given in Table 2.3.

Table 2.3 Spectral vegetation indices and formulas tested for model optimization in support vector machine and random forest machine learning classifiers

GCI (Green Chlorophyll Index) Gitelson et al. (2005)	$\frac{\text{NIR}}{\text{Green}} - 1$
MSRE (Modified Simple Ratio Red-Edge) Cao et al. (2013)	$\frac{\left(\frac{\text{NIR}}{\text{Red edge}}\right) - 1}{\sqrt{\left(\left(\frac{\text{NIR}}{\text{Red edge}}\right) + 1\right)}}$
MSR (Modified Simple Ratio) Chen (1996)	$\frac{\left(\frac{\text{NIR}}{\text{Red}}\right) - 1}{\sqrt{\left(\frac{\text{NIR}}{\text{Red}}\right)} + 1}$
GNDVI (Green Normalized Difference Vegetation Index) Gitelson et al. (1996)	$\frac{\text{NIR} - \text{Green}}{\text{NIR} + \text{Green}}$
NDRE (Normalized Difference Red-Edge) Barnes et al. (2000)	$\frac{\text{NIR} - \text{Red edge}}{\text{NIR} + \text{Red edge}}$
GRVI (Green Red Vegetation Index) Tucker (1979)	$\frac{\text{Green} - \text{Red}}{\text{Green} + \text{Red}}$
TGI (Triangular Greenness Index) Hunt et al. (2013)	$\frac{\left(120 * (\text{Red} - \text{Blue})\right) - \left(190 * (\text{Red} - \text{Green})\right)}{2}$
NDVI (Normalized Difference Vegetation Index) Rouse et al. (1974)	$\frac{\text{NIR} - \text{Red}}{\text{NIR} + \text{Red}}$
RECI (Red-Edge Chlorophyll Index) Gitelson et al. (2005)	$\frac{\text{NIR}}{\text{Red edge}} - 1$
OSAVI (Optimized Soil Adjusted Vegetation Index) Rondeaux et al. (1996)	$\frac{\text{NIR} - \text{Red}}{(\text{NIR} + \text{Red} + 0.16) * (1 + 0.16)}$
SAVI (Soil Adjusted Vegetation Index) Huete (1988)	$\frac{\text{NIR} - \text{Red}}{(\text{NIR} + \text{Red} + 0.5) * (1 + 0.5)}$
MGRVI (Modified Green Red Vegetation Index)	$\frac{\text{Green} - \text{Red}}{\text{Green} + \text{Red}} + \text{NIR}$

2.8 Hemp model training and testing

Training data were generated in ArcGIS Pro as described in section 2.4. Selection of pixels which showed '*Botrytis*-infected inflorescence', 'healthy inflorescence', 'unhealthy leaves', and 'healthy leaves' consisted of 1853, 1443, 2734, and 13,711 identified pixels, respectively. Pixel classes were determined based on false color images of vegetation indices and spectral bands show distinctions between digital numbers. A composite raster containing all five bands and 12 vegetation indices was exported from ArcGIS Pro and uploaded to RStudio along with training data polygons. Training polygons were used to extract the digital numbers of each of the 17 bands or vegetation indices found within those regions. Pixel values for each band or vegetation index were normalized on a scale of 0 to 1 using the formula: (x-min(x)) / (max(x) - min(x)). Outliers were then identified and removed from each of the four training groups using the formula: (quantile 1 - 1.5 × interquartile range) × (quantile 3 + 1.5 × interquartile range). Finally, the four training groups were randomly sampled down to 1400 values per band for '*Botrytis*-infected inflorescence' and 'healthy inflorescence' and 2500 values per band for 'unhealthy leaves' and 'healthy leaves' for a total of 7800 digital numbers per band across the four training groups. Data were partitioned into 70% training and 30% testing data. The training data set was then visually assessed at each spectral band in a box and whisker plot to initially determine if digital number differences were captured within specific bands or vegetation indices. Bands and vegetation indices were analyzed in an ANOVA, Mean Decrease Gini using a random forest (Liaw and Wiener 2002; Han et al. 2016), and a pairwise t-test of means with a Bonferroni adjustment. Mean Decrease Gini is essentially a measure of variable importance for estimating a determined variable. Bands or vegetation indices which showed no statistical difference between any of the two groups or had a large overlap in digital numbers were dropped from the model. Values low in the Mean Decrease Gini were also removed.

During the first phases of model creation, SVM (Meyer et al. 2020) and Random Forest (RF) (Breiman 2001; Liaw and Wiener 2002) were used. Sets of bands and vegetation indices selected as variables based on univariate statistics and combined into SVM models which were optimized by adjusting the cost and gamma. The same variables combinations were used in the RF model and the number of trees and number of splits at each node were adjusted to optimize the RF model. The 30% subset of the data held out was used to test the various models. A cycle of model parameter tuning, band combinations, and machine learning model options were conducted in pursuit of a model with the greatest balance of accuracy, specificity, sensitivity, and reduced variables. A new vegetation index composed of the previous GRVI (Green-Red Vegetation Index) spectral index and NIR was created, and named Modified Green-Red Vegetative Index (MGRVI) (Table 2.3). The digital numbers of 'healthy leaves', 'healthy inflorescence', and 'unhealthy leaves' were merged into one class, thus creating a binary classification of '*Botrytis*-infected inflorescence' and all other plant tissue. The training data set used for the final model was comprised of 4,513 pixels of 'healthy inflorescence', 'healthy leaves', and 'unhealthy leaves', now referred to as 'other plant tissue', and 947 '*Botrytis*-infected inflorescence' pixels. The model was tested with 30% of partitioned test data which was 1,887 pixels of 'other plant tissue' and 453 pixels of '*Botrytis*-infected inflorescence'. A confusion matrix was used to assess the model's accuracy along with the associated statistics described in section 2.5. Other packages used in R included 'rgdal' (Bivand et al. 2020) and 'raster' (Hijmans 2020), along with base R (R Core Team 2013) to upload, visualize, and manipulate raster data.

2.9 Hemp model validation

Further confirmation of the model's ability to classify outside of the selection of pixels in the model training data set was conducted by applying the generated SVM model to hemp plants extracted from the background of soil and vegetation, because it provided the greatest accuracy, sensitivity, specificity compared to the RF

model. The digital elevation model was converted to a canopy height model (Zhang et al. 2016; Roussel and Auty 2020; Roussel et al. 2020) by subtracting the canopy height from the ground in RStudio and exported as a raster to ArcGIS Pro. The NDVI raster in ArcGIS Pro was used for the segmentation function, which is dictated by three parameters: spectral detail, spatial detail, and the minimum segment size, which were set to 15.5, 9, and 5000, respectively. A mask was then applied to this segmented image to remove the background vegetation and soil. This newly segmented image, along with the canopy height model, were stacked and an intersection was applied that generated a layer which only included regions that overlapped on both layers (canopy height model and segmented NDVI) of polygons. Finally, a buffer was added that shrank these polygon regions inwards the equivalent of 8 pixels to ensure no background data were included in the analysis. These polygons were exported from ArcGIS Pro and imported into RStudio where they were used to extract the plants from the background soil and vegetation. Upon extraction of the plants, the SVM model was used to classify all the pixels of the hemp plants within the plots. A threshold of greater than -3000 in Triangular Greenness Index (TGI) was applied to pixels that were classified as '*Botrytis*-infected inflorescence' and converted them to the 'other plant tissue' class. The raster for each plot was then exported and uploaded to ArcGIS Pro for visualization and sampling.

Three disease incidence rating methods were used for comparison in the final assessments. The first method used was the *field-based* strategy, which is the conventional method of data collection derived from on-the-ground sampling. The next two include the *classified model* and the *reference false color images*, both of which came from remotely sensed data from aerial collection on the 9 Oct flight. The *classified model* was the output raster identifying pixels classified as either 'diseased' or 'non-diseased', based on the SVM model and TGI thresholds. The *reference false color images* was a visual assessment of the collected images using the MGRVI, NDVI, and TGI spectral indices to rate inflorescence "by hand" as either 'diseased' or 'non-diseased' and served as a reference for comparison to the *classified model*. This was necessary to determine if the pixels were either correctly or incorrectly classified

by the *classified model*. Sampling of the *classified model* pixels within the hemp plants were conducted using the same methodology as field sampling. The same five plants within each plot used for an in-field visual assessment were used for remotely sensed aerial image analysis, and eight inflorescences were randomly selected per plant. Visual appearance of pixels within inflorescence using the reference images allowed for identification inflorescence as ‘diseased’ or ‘non-diseased’ and were then compared with the *classified model*’s predictions as ‘diseased’ or ‘non-diseased’ to estimate disease incidence in the field through remote sensing. A threshold of 4 pixels within an inflorescence identified as ‘diseased’ or ‘non-diseased’ was used as the minimum number of pixels to characterize the prediction as an accurate classification by the model. By setting the threshold too low, the model may return too many false positives. Alternatively, a threshold too large may result in an issue with increased number of false negatives. The binary classification of both the disease detection through the *reference false color images* utilizing the MGRVI, NDVI, TGI spectral indices and the *classified model* prediction was analyzed as incidence data with a generalized linear mixed model assuming a binomial distribution of the response variable. Treatment was the fixed effect with replicate block as a random effect. Analyses were conducted using the GLIMMIX procedure in SAS version 9.4. Reference data from MRGVI and the classification of the model were assessed in a confusion matrix for insights to accuracy, false positives, false negatives, specificity, and sensitivity. Lastly, the incidence data for each treatment of each block were plotted on a graph for comparison of all the sampling methods and fitted with a line of best fit and associated R-squared value.

Chapter 3: Results

3.1 Classification and assessment of black leg on turnip

A clear division was observed between the '*Leptosphaeria*-affected' (diseased) and 'healthy plant tissue' (non-diseased) pixels (Figure 3.1). A total of 34 support vectors were used to determine a hyperplane for the binary classification of pixels when applying the SVM model with a Gamma = 0.1 and cost = 1.

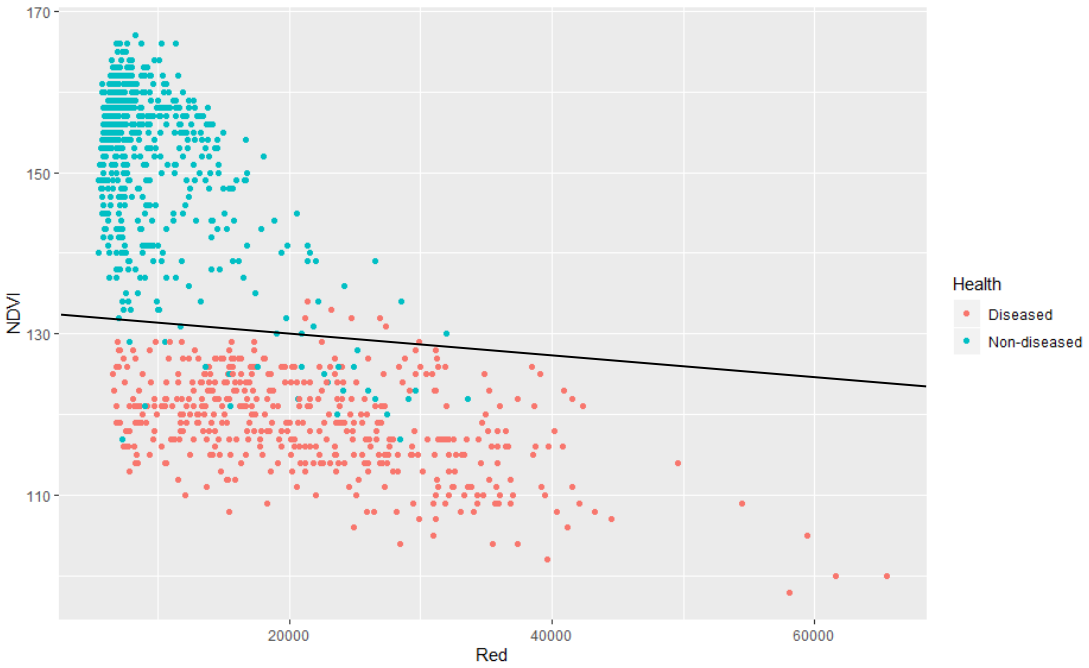

Figure 3.1 A plot of pixels used in the training data set to determine the hyperplane of the SVM model with hyperplane drawn through the training data using 34 data points as support vectors. When testing data are used, points below the line will be classified as 'diseased', while pixels above will be classified as 'non-diseased'.

Of the 676 total pixels tested in the model, 96.8% were accurately classified as either diseased or non-diseased, while 3.2% were misidentified as either false positives or false negatives, 0.04 and 0.03, respectively. The model obtained a reported specificity of 0.96 and a sensitivity of 0.97

Table 3.1 Confusion matrix of black leg-turnip model for 676 pixels by a SVM model

	Reference	
Prediction	**Diseased tissue**	**Non-diseased tissue**
Diseased tissue	0.97	0.04
Non-diseased tissue	0.03	0.96

The final assessment of the SVM binary classifier was confirmed with classification of four individual leaves containing 15,519 pixels (Figure 3.2). Classification of pixels in the four leaves resulted in an average accuracy of 97.0% and a Kappa coefficient of 0.60 (Table 3.2). The specificity was 0.99 and sensitivity was 0.48.

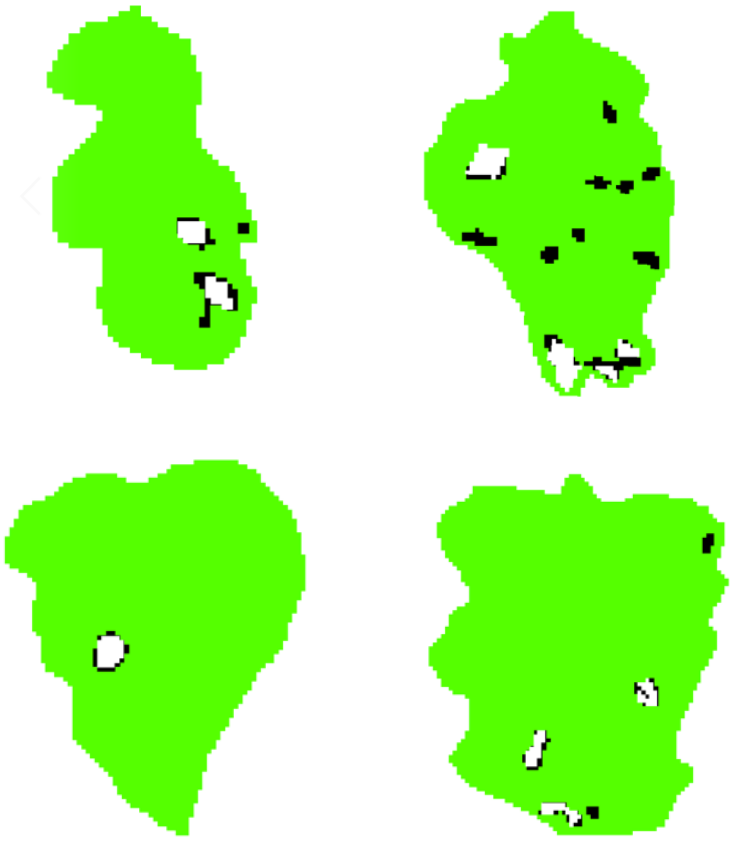

Figure 3.2 Four turnip leaves removed from background with pixels classified as either ‘non-diseased’ (green) or ‘diseased’ (white). The black-colored pixels indicate pixels that were manually selected as ‘diseased’, true positives that were misclassified by the SVM model.

Table 3.2 Confusion matrix of black leg-turnip model on four turnip leaves consisting of 15,519 pixels by SVM

	Reference	
Prediction	**Diseased tissue**	**Non-diseased tissue**
Diseased tissue	0.48	0.01
Non-diseased tissue	0.52	0.99

3.2 Classification and assessment of gray mold on hemp

A generally high rate of ‘unhealthy leaf’ pixel misidentification by all models tested led to the development of a novel vegetation index, MGRVI. Initially, differences in the four training classes for each spectral band and vegetation index were assessed for relatedness in pixel ranges and overlap with an emphasis on the minimum and maximum values. Means of classes were less significant than large overlaps in range regarding SVM and RF classification models. Box and whisker plots of the MGRVI with outliers included (Figure 3.3) or removed (Figure 3.4) are visualized below and were used for the hemp-gray mold model development. With the outliers included, the maximum value for ‘*Botrytis*-infected inflorescence’ (unhealthy bud) was 0.91 and the minimum for ‘unhealthy leaves’ was 0.38, for a difference of 0.53 in digital number values. With outliers removed, the maximum value for ‘*Botrytis*-infected inflorescence’ (unhealthy bud) was 0.64 and the minimum value for ‘unhealthy leaves’ was 0.54, for a difference of 0.10 in digital number values. By merging ‘healthy inflorescence’, ‘unhealthy leaf’, and ‘healthy leaf’, no differences in minimums and maximums are seen because ‘unhealthy leaves’ represent the lowest values in the merging of these three classes.

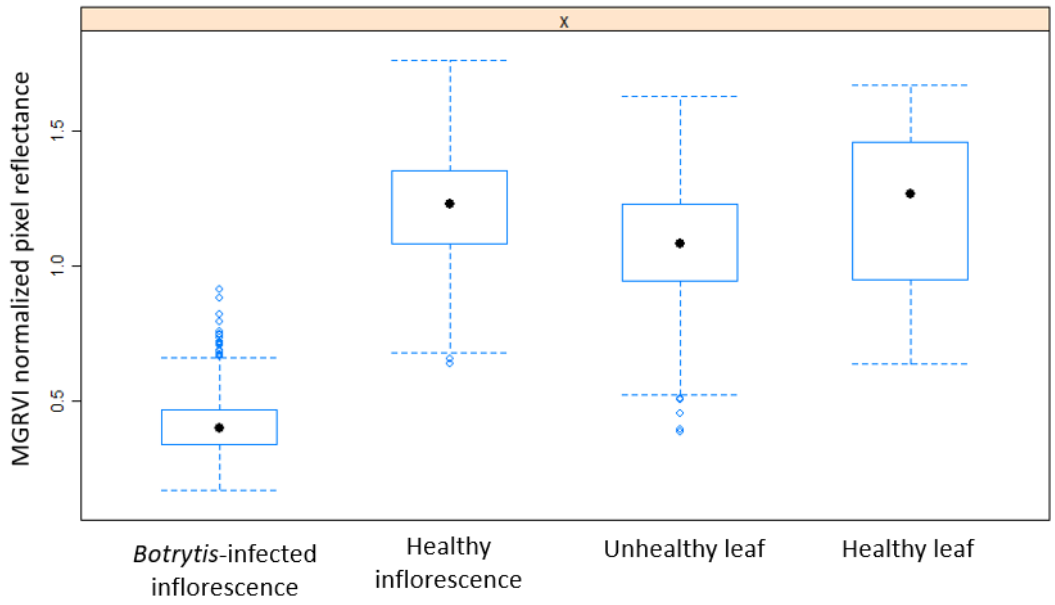

Figure 3.3 The box and whisker plot of gray mold on hemp training data of MGRVI pixels with outliers included in the four training classes.

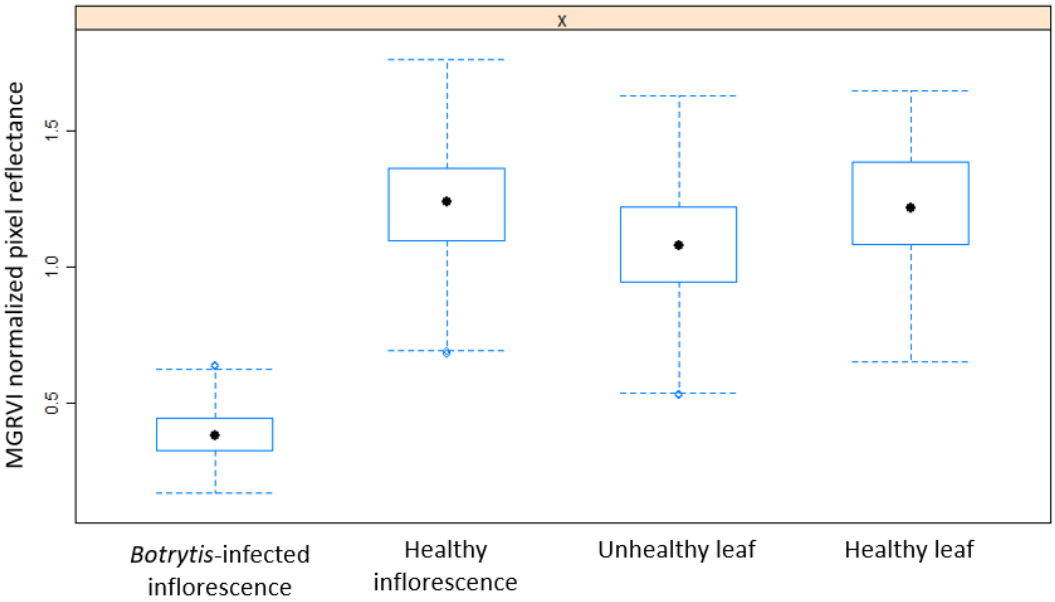

Figure 3.4 The box and whisker plot of gray mold on hemp training data of MGRVI pixels with outliers removed from the four training classes.

The set of bands and vegetation indices were additionally tested for differences by an ANOVA when looking at data with four classes and were then further assessed with a pairwise t-test of means adjusted by Bonferroni. This analysis helped to remove vegetation indices or bands where there were no significant differences in observed means and would not have contributed significantly to the model's ability to classify training groups. With two classes, an ANOVA was conducted using MGRVI, a significant difference was seen between classes ($P < 0.01$). Mean Decrease Gini was used as a final assessment in determining variable importance and what should be used for the hemp-gray mold model. Bands or vegetation indices with greater Mean Decrease Gini values are associated with contributing to a better model fit. Table 3.3 lists the significance given to each variable for both classes, '*Botrytis*-infected inflorescence' and 'other plant tissue', in addition to the four classes that include '*Botrytis*-infected inflorescence', 'healthy flowers', 'unhealthy leaves', and 'healthy leaves'. The MGRVI was the most important variable for the two classes and was subsequently, the sole variable selected for the final gray mold-hemp model.

Table 3.3 Mean Decrease Gini values associated with each band or vegetation index when assessing variables with two training classes and four training classes

Band or vegetation index	**Mean Decrease Gini (2 classes)**	**Mean Decrease Gini (4 classes)**
SAVI	76	478
OSAVI	85	490
RECI	6	31
GCI	32	237
MSRE	7	37
MSR	87	507
GNDVI	25	271
NDRE	7	40
NDVI	86	438
GRVI	336	260
TGI	257	384
MGRVI *	430	315
Red edge	30	47
Red	7	167
Near-infrared	37	50
Green	48	178
Blue	8	35

*MGRVI was the selected variable for the gray mold-hemp SVM model.

The final gray mold-hemp model utilized an SVM of Gamma = 1 and cost = 1 with the new vegetation index, MGRVI, which was determined to provide the greatest balance of accuracy with the fewest variables included. The SVM model used 91 support vectors and resulted in an accuracy of 99.15% and a Kappa value of 0.97 with a sensitivity of 0.97 and a specificity of 0.99 (Table 3.4).

Table 3.4 Confusion matrix of a gray mold-hemp model for 2,340 classified testing pixels by SVM

	Reference	
Prediction	***Botrytis*-infected inflorescence**	**Other plant tissue**
Botrytis-infected inflorescence	0.97	0.01
Other plant tissue	0.03	0.99

Field validation of the SVM model indicated misclassification of ‘unhealthy leaves’ as ‘*Botrytis*-infected inflorescence’. Due to many false positives of ‘unhealthy leaves’, another step was added to the analysis to reduce pixels falsely identified as ‘*Botrytis*-infected inflorescence’ to ‘other plant tissue’. This post-SVM step used TGI to help optimize the accurate designation of pixel classification creating an iterative process. The differences between classes of pixels in the TGI, with and without outliers, are seen below in Figures 3.5 and 3.6, respectively. With the outliers included, the maximum value for ‘*Botrytis*-infected inflorescence’ was -680 and the minimum for ‘unhealthy leaves’ was -13,855, for a difference of over 13,000 in digital number values. With outliers removed the maximum value for ‘*Botrytis*-infected inflorescence’ was -680 and the minimum value for ‘unhealthy leaves’ was -3065 for a difference of 2385 in digital number values. A threshold of -3000 was determined to be effective at correcting for false positives of ‘unhealthy leaves’ and was included in the analysis, which changed ‘*Botrytis*-infected inflorescence’ with a digital number greater than -3000 to ‘other plant tissue’. An example of the intersection between canopy height model, segmented NDVI, and 8 pixels buffer is illustrated in Figure 3.7. Each SVM classified plot with the TGI threshold can be seen in Figure 3.8, along with an individual plant.

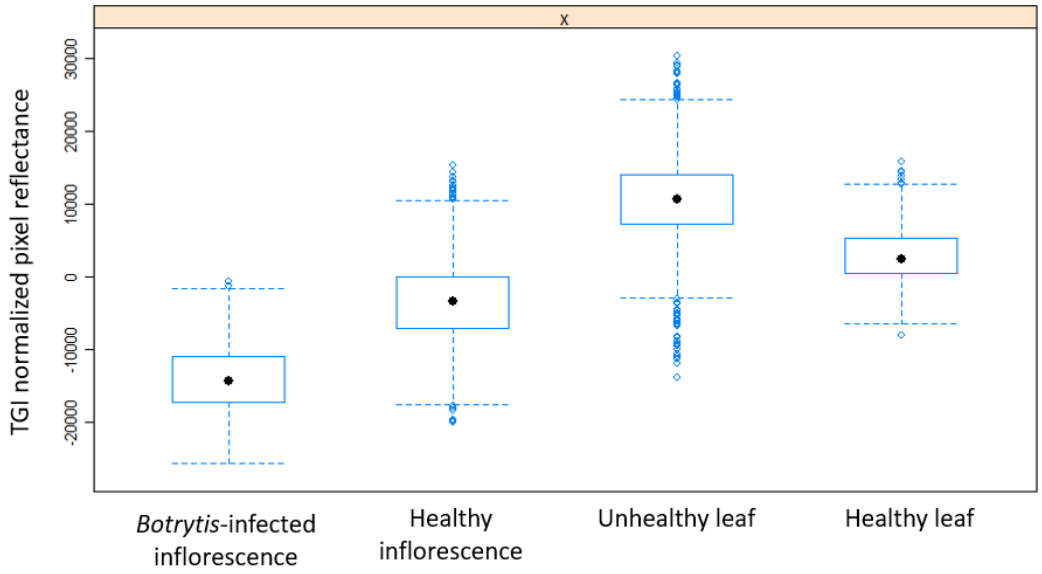

Figure 3.5 The box and whisker plot of gray mold on hemp training data of TGI pixels with outliers included in the four training classes.

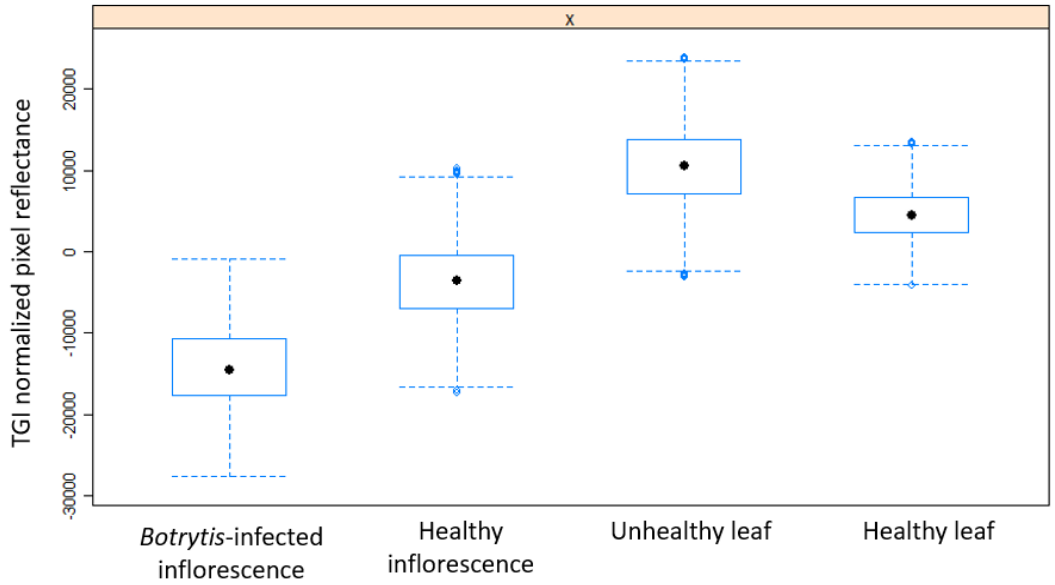

Figure 3.6 The box and whisker plot of gray mold on hemp training data of TGI pixels with outliers removed from the four training classes.

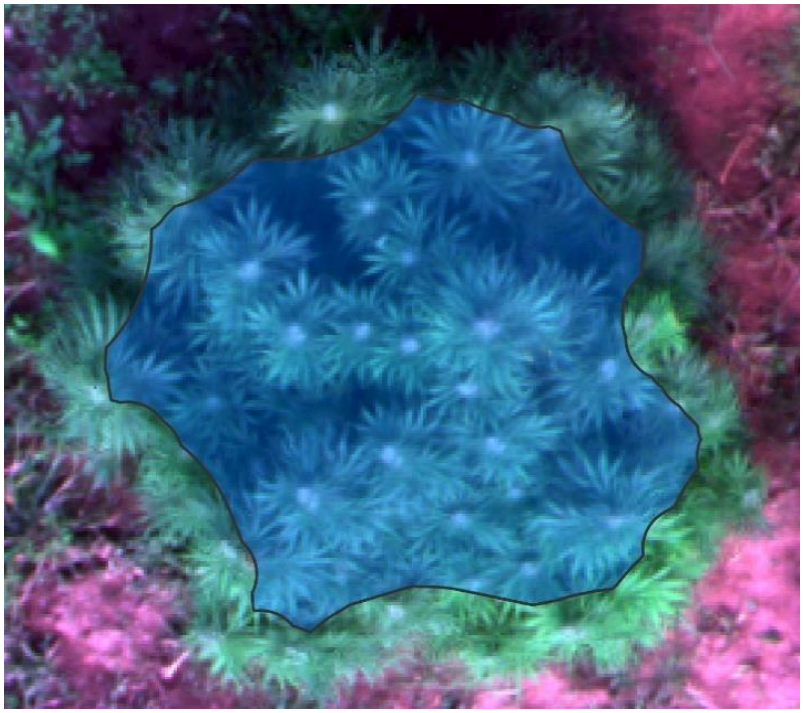

Figure 3.7 Hemp plant with blue polygon indicating the region being extracted through the overlap of ArcGIS Pro segmentation function, canopy height model, and 8-pixel buffer.

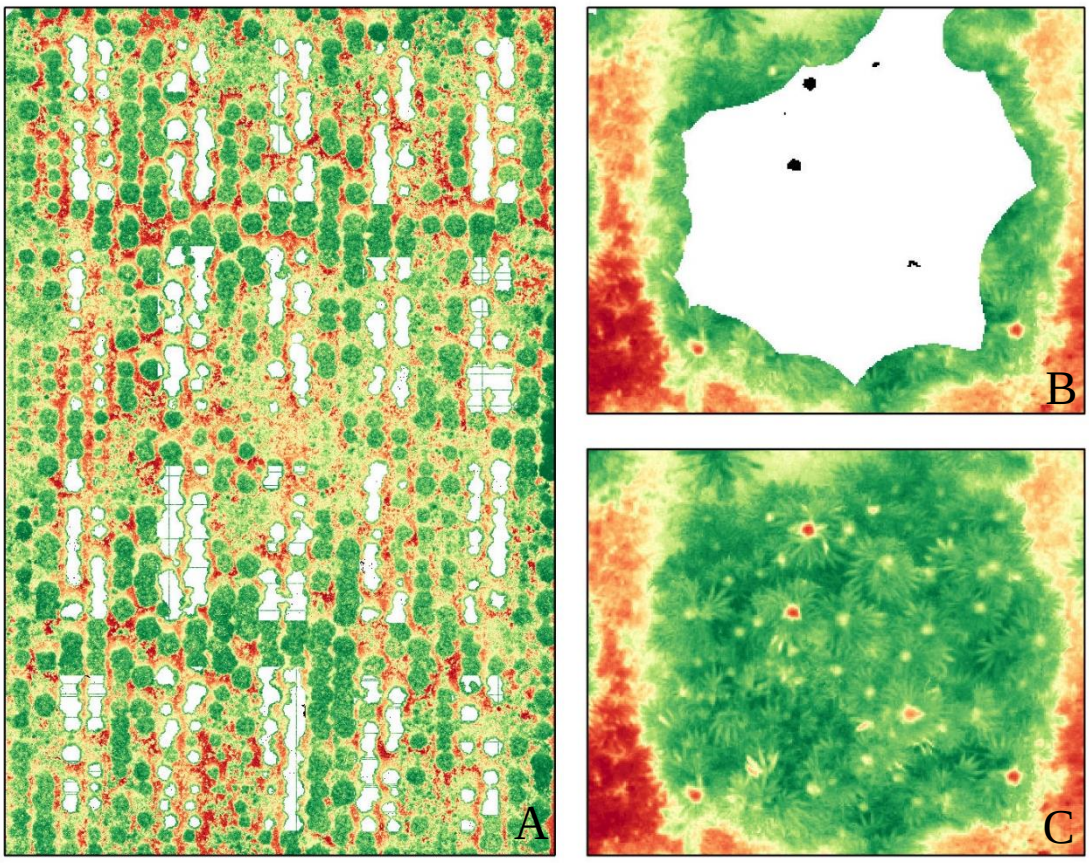

Figure 3.8 An NDVI false color image of a hemp field at the Oregon State University Botany and Plant Pathology Field Laboratory with extracted plant polygons in white for each treatment plot (A). An individual plant with white pixels identifying healthy plant tissue and black identifying *Botrytis*-infected inflorescence (B). The hemp plant from image B without identified pixels as an NDVI false color image with red pixels indicating disease within the plant (C).

The sampling of hemp inflorescence pixels from the *classified model* derived from the SVM model and TGI threshold had a 95.8% accuracy, with a Kappa of 0.80. The specificity was found to be 0.99 and the sensitivity was 0.70 (Table 3.5).

Table 3.5 Confusion matrix of 800 classified inflorescences by the SVM and TGI gray mold-hemp model from each plot of a hemp field at the Oregon State University Botany and Plant Pathology Field Laboratory

	Reference	
Prediction	***Botrytis*-infected inflorescence**	**Other plant tissue**
Botrytis-infected inflorescence	0.70	0.01
Other plant tissue	0.30	0.99

ANOVA indicated significant treatment effects assessed using *field-based* disease incidence (the conventional on foot disease assessments) ($P \leq 0.0001$), *classified model* rating disease incidence ($P = 0.0885$), and *reference false color images* disease incidence ($P = 0.0289$). Inflorescence in the nontreated control had the greatest estimated percentage of gray mold using each assessment method (Table 3.6). However, the mean percentage of gray mold incidence for all treatments was much larger in *field-based* ratings than in either the *classified model* or the *reference false color images* disease rating method. The mean incidence percentage of gray mold rankings between the *classified model* and the *reference false color images* disease assessments were found to be the same. Significant differences between nontreated control and the three fungicide treatments were observed in both *field-based* incidence and *reference false color images* incidence ($P \leq 0.05$). The rank order of mean incidence between the *field-based* rating method versus the *classified model* method differed between plants in plots that received treatment 1 and 2, but means were not found to be significantly different for either treatment.

Table 3.6 Gray mold incidence on hemp inflorescence for the *field-based*, *classified model*, and *reference false color images*-based disease assessment methods

	Gray mold incidence (%)		
Treatment	**Field-based [X]**	**SVM classified model [Y]**	**Reference false color images [Y]**
Nontreated control	83.1 a[Z]	17.6 a	23.6 a
Treatment 1	59.1 b	6.6 ab	9.9 b
Treatment 2	58.0 b	7.5 ab	11.7 b
Treatment 3	55.5 b	5.4 b	9.5 b

X *Field-based* data rating and collected was conducted on 9 Oct 2020.

Y Remote sensed data was collected on 7 Oct 2020 for both *classified model* and *reference false color images* disease assessment methods.

Z Means within the same column followed by the same letter are not significantly different based on a generalized linear mixed effects model and pairwise t-test at $P \leq 0.05$.

Field-based incidence ratings, *classified model* incidence ratings, and *reference false color images* incidence rating were plotted for each treatment at each block. Incidence ratings from the *classified model* ratings had a low R-squared at 0.26, when regressed against disease incidence using *field-based* assessments (Figure 3.9). Incidence ratings from the *reference false color images* and *field-based* disease assessments were found to also have a low R-squared value of 0.32. Disease assessment ratings from the *classified model* ratings were found to have the highest R-squared correlation with *reference false color images* disease ratings of 0.85.

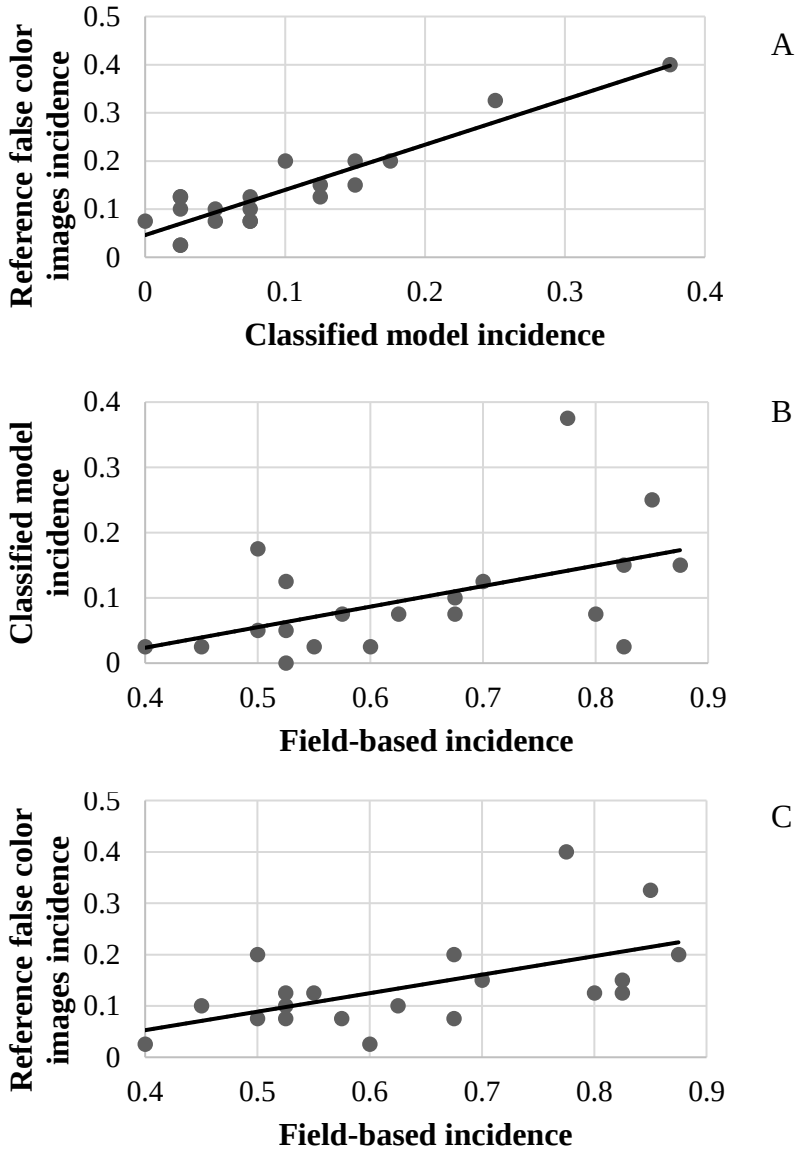

Figure 3.9 Gray mold incidence for four treatments with five replicates by two disease assessment methods and a third disease assessment using by-hand classification of false color images. The conventional field-based and the *classified model* that utilizes an SVM and TGI threshold was regressed. (R-squared = 0.26) (A). The field-based and *reference false color images* disease incidence regression (R-squared = 0.32) (B). The *classified model* and the *reference false color images* disease incidence regression (R-squared = 0.85) (C).

Chapter 4: Discussion

Classic field scouting techniques for pathogen identification and disease incidence quantification can be subjective and time-consuming. Furthermore, scouting on foot can be destructive to the plant, costly, and burdensome, especially during the rainy season (Barbedo et al. 2016). Traditionally, fungicide application programs treat pest pressure with a homogenous pesticide application rather than localized applications based on disease presence (West et al. 2003; Mahlein et al. 2012). Remote sensing techniques can provide an alternative to traditional field sampling, resolving many of these concerns through an objective approach to sampling and provide more insightful IPM programs required for agricultural efficiency going into the future.

The results of this research indicate that both black leg on turnip and gray mold on hemp can be accurately identified through remote sensing with a multispectral sensor and machine learning techniques. The development of a novel vegetation index, MGRVI, was necessary and reveals differences in reflectance values for hemp pixel classes not seen in the other bands or vegetation indices. However, this study indicates that a high accuracy of pixel classification with few false negatives and positives does not directly translate to dependable disease identification in field-based applications. Although estimated disease incidence was much lower in the *classified model* compared with the *field-based* ratings, ranking of treatment means by both methods were found to be similar. While rankings were similar at the experimental level, a low correlation between disease incidence ratings were found for each treatment plot when comparing the two methods. This research is the first report on detection of gray mold on hemp under field conditions, while Ferentinos et al. (2019) was able to detect gray mold on hemp in a greenhouse where other abiotic and biotic factors were present. This thesis research is also the first to report on detecting black leg on a *Brassica* crops. Others have identified leaf spot diseases on similar plants such as Cercospora leaf spot on sugar beet (Zhou et al.

2014) using a multispectral camera while Mahlein et al. (2010) detected Cercospora leaf spot on sugar beet with a SVM and a hyperspectral camera. This thesis work contributes to the current literature by broadening our understanding of methods that can be used for remotely sensed disease detection. It also provides a novel vegetation index for disease detection which may be of use in detecting disease in other host-pathogen systems. The detection of gray mold on hemp case study also presents an alternative technique to traditional methods of disease detection.

Because SVM models use support vectors to generate a hyperplane, understanding the range of data is more useful than comparing means. Box and whisker plots provide a clear visual depiction of the data spread along with the outliers, which tend to define the model's hyperplane, particularly for an SVM. In many pixel-based analyses using machine learning, outliers are not removed from the training classes, but this approach of removing outliers has seen acceptance in other fields due to increased model accuracy (Maniruzzaman et al. 2018). Outliers were removed from this model for two reasons. Firstly, when generating a training data set, a limited number of misclassified pixels is not unexpected. If the data set is extremely large, these misclassified pixels have less of an impact on the generated hyperplane. Secondly, machine learning model building should utilize a cyclic process of model creation, repeated testing and fine-tuning of the model, until the best results are found. Through this repetition of model creation and testing, the removal of outliers provided a hemp-gray mold model with the best results with the data used as indicated in the confusion matrix. Pixels designated as outliers in the hemp model were found to be primarily pixels displaying very low levels or early stages of disease, or were chlorotic or necrotic leaves that visually appeared as gray mold-affected inflorescence through the values of the MGRVI data.

The black leg-turnip model did not utilize outlier removal, adhering to a more conventional machine learning model development method set. In the turnip training data set, overlap occurred with 'non-diseased' pixels merging into the 'diseased' cluster of pixels. This same problem arose in the training data set for '*Botrytis*-

infected inflorescence' and 'other plant tissue'. This could be a result of genuine overlapping of reflective values between the diseased and non-diseased classes, an imperfect training data set, outliers, or an insufficient number of training values used in the model. As mentioned earlier, obtaining data points of the highest accuracy and precision as possible when generating a training data set is essential to creating a robust classification model with an SVM, and removal of outliers can be conducted at the user's discretion to reduce overlap of classes. Although there is overlap, a clear distinction existed between the two training classes in both data sets and the distinction is supported by SVM models containing a high accuracy, specificity, and sensitivity for both case studies during validation using the test data.

The results of the SVM models developed for black leg on turnip and gray mold on hemp appear to be sufficient for *ex situ* applications based on the model validation findings using the test data. For further model validation, hemp plants and individual turnip leaves were extracted. Extraction of the hemp plants from the background noise such as brown-colored soil and weedy vegetation was one of the greater challenges of this portion of the remote sensing work with hemp, but can be accomplished through various means (Hamuda et al. 2016). To carry out extraction of the hemp plants from the field site used in our study, conservative methods were applied which removed the outer edge of most plants to ensure that little to none of the soil appeared in the analysis, as soil generally shows up as false positives. While not all of the pixels composing the plant were included in the final analysis, a large enough region of most plants were extracted for a representative sampling of the field. Unless the outer edges of the plants display more disease than the inner portion, which did not appear to be the case in this field site, this conservative approach to plant canopy extraction seems acceptable as a work around for the problems posed by exposed soil and other vegetation surrounding individual plants. However, the noise caused by soil and vegetation in this field that led to misclassification of pixels, may be less of an issue in commercial hemp fields that utilize black plastic within the plant rows. Because only the turnip leaves were manually extracted, rather than entire plants, false negative and positives were much less common, as would be expected. If

whole turnip plants were extracted, similar issues as posed by the hemp field would likely arise, making the classification process more difficult. Nonetheless, for any agricultural field-based application, extraction of the plants from the background is pertinent to obtaining accurate and meaningful analysis results.

For application of this technology under field conditions, a much lower level of false negatives is necessary to make this remote sensing tool reliable. Through visual assessment of the classified pixels in the raster, it was clear that some of the false positives appearing on the hemp image were due to necrotic and/or chlorotic foliage rather than *Botrytis*-infected inflorescence. This tends to be a reoccurring issue and is one of the greatest challenges of this work; it is an anticipated problem when using field data rather than greenhouse or lab-grown plants free of other abiotic and biotic factors influencing or mimicking plant health and appearance of yellowing or browning plant tissues.

TGI showed the least amount of overlap between the classes, ‘unhealthy leaves’ and ‘B*otrytis*-infected inflorescence’ among bands and vegetation indices examined. The maximum and minimums of both these classes, analyzed with and without outliers, were used to determine the threshold of -3000 to transfer pixels assigned to the ‘B*otrytis*-infected inflorescence’ class to the ‘other plant tissue’ class. This threshold resulted in fewer false positives, and while the inclusion of the threshold did slightly increase the occurrence of false negatives, the impact of including the threshold was important enough for it to be part of the final model used for field testing.

In determining how the SVM model classified pixels, in some cases, 1, 2, or 3 pixels were correctly classified as ‘*Botrytis*-infected inflorescence’ but were not counted because 4 pixels was considered the minimum number of pixels necessary for classification as a ‘*Botrytis*-infected inflorescence’. Lowering this threshold may have slightly influenced the results but only to a small degree. The SVM model and TGI threshold resulted in a high overall accuracy but low sensitivity, which is thought to be influenced partly by the TGI threshold. Many of pixels changed by the threshold

were indicating either early signs or symptoms of the disease or contained a mix of diseased and non-diseased pixels. Thusly, this model did not have optimal classification capabilities needed to classify pixels that were in early stages of disease development or were a mosaic of diseased/healthy pixels. This was confirmed through visual assessment during classification, where slightly diseased inflorescences in false color images (NDVI and MGRVI) appeared faintly red, whereas very diseased inflorescences appeared deep red.

The final determination was comprised of comparison of the SVM and TGI pixel classification model (*classified model*) and the conventional disease assessments (*field-based*) for measuring gray mold incidence on hemp. While there was general agreement amongst both sampling strategies that the greatest disease incidence was observed in the nontreated control and lowest incidence was found in Treatment 3, the middle two ranked treatments, Treatments 1 and 2, had alternating rankings. Despite this switch, the means were not found to be significantly different. The disease incidence estimates seen in the *classified model* were found to be much lower percentages than what was observed in the *field-based* disease assessments. This likely comes from the inability to detect disease symptoms or signs that aren't visible from directly above the plant (nadir perspective), e.g., disease lower down the length of the inflorescence goes unseen when assessments are done by an UAV. The classical *field-based* sampling assessed disease along the upper 30-cm length of the inflorescence, while the data used in the *classified model* most likely contained only the uppermost portions of each inflorescence and did not capture the sides or entirety of the 30-cm region. The nadir perspective of the aerial flights is one of the greatest challenges associated with remote disease detection via UAV for this reason. Aerial remote sensing was also conducted 48 hours later than the ground sampling disease incidence measurements were taken. During this 48-hour period, disease incidence likely increased and could have resulted in truly different levels of disease incidence, so the time differential may account in part for the lower incidence ratings found in the *classified model* versus the *field-based* results but due to large differences in treatment means between these two methods, it is highly unlikely that the time

difference accounted for most of the treatment means disparity. Additionally, as previously observed, the *classified model's* sensitivity was too low to detect all signs or symptoms of *Botrytis* that were present. Disease observed through assessments utilizing the *reference false color images* of the same inflorescences used in the *classified model* rating, was found to be slightly higher, but means generated by the *reference false color images* were still much lower than *field-based* disease assessments. Both the *classified model* assessment of disease incidence and the *reference false color images* incidence had the same ranking of treatments. This indicates that although the *classified model* may have a low sensitivity, an increased sensitivity and associated decrease in false negatives would not have changed the rankings of gray mold incidence seen among the fungicide treatments. While the rankings were the same among the *reference false color images* and the *classified model*, the *reference false color images* showed a significant difference between nontreated control and the three biofungicide treatments while the *classified model* did not find a significant difference between nontreated and the three biofungicide treatments. This indicates that if the *classified model* had perfectly classified all hemp inflorescences, resulting in 100% overall accuracy and the equivalent to the *reference false color images*, the significance differences observed among treatments would have been the same as those found in the *field-based* assessment method.

The comparison of disease incidence ratings for *field-based* assessment and the *classified model* resulted in a low R-squared value, which suggests there are large differences in incidence ratings between these two assessment strategies for each treatment plot. The R-squared is slightly increased in the comparison of the *reference false color images* disease ratings with *field-based* disease incidence assessment, but overall, both the *classified model* and the *reference false color images* ratings have a poor fit when compared with the *field-based* data. Mean disease incidence percentages for *field-based* rating in comparison to the other two methods shows large differences among treatments, but also they largely differ within each plot. Conversely, the *reference false color images* rating compared with the *classified model* rating for disease incidence resulted in a high R-squared value. This stronger

relationship is not unexpected since both methods utilized the same aerial images captured by the drone. Both of these remote sensing disease assessment methods, *reference false color images* and the *classified model*, had a less than ideal comparison to the *field-based* assessment, reinforcing that hemp gray mold incidence data collected aerially via remote sensing failed to capture the proportional percentage of disease incidence present that was detected by *field-based* disease assessment techniques.

The remote sensing methods reported in this research were similar to what other researchers have reported in other pathosystems. The gray mold-hemp and black leg-turnip case studies utilized a similar methodology as outlined by Abdulridha et al. (2019), which consists of image acquisition, pre-processing, image segmentation, feature extraction, and classification. These steps are generally the standard framework for many remote sensing and model building processes. Image acquisition in our research fell towards the lower end of flight/image acquisition elevation, at 10 m above ground level for detection of gray mold in hemp and 1.5 m for black leg in turnip. Abdulridha et al. (2019) also collected images for detection of laurel wilt in avocado at 10 m but they were not collected via UAV. Similar to the turnip image acquisition case study, Dammer et al. (2011) acquired imagery at 2.4 m above wheat plants with Fusarium head blight, while images have been taken as low as 25 cm from the plant (Bravo et al. 2003). Others have conducted flights at 120 m above ground level (Albetis et al. 2017) with limited success, and successfully at 40 m above the ground (Heim et al. 2019), based on overall accuracy assessments. While there are many factors that come into consideration which ultimately dictate the flight parameters, increased imagery collection elevations that maintain accuracy should always be a goal.

The gray mold on hemp case study utilized a SVM along with a binary threshold parameter to classify pixels. While we chose not to use the random forest classifier, Heim et al. (2019) while looking at Myrtle rust on lemon myrtle, had a high overall classification accuracy, suggesting it is a viable machine learning model

option but likely dependent on crop and pathogen. Alternatively, Abdulridha et al. (2019) used both a neural network multilayer perceptron and K-nearest neighbor. The neural network proved to be more effective than the K-nearest neighbor, and this is generally true when supervised machine learning or deep learning models are used in comparison to unsupervised. While machine learning models have been a staple of pixel-based classification in the recent years (Sandino et al. 2018; Abdulridha et al. 2019; Heim et al. 2019), deep learning models are now becoming more popular (Mohanty et al. 2016; Ramcharan et al. 2017; Ferentinos 2018; Ferentinos et al. 2019; Saleem et al. 2019). Prior to either of these classification techniques, unsupervised classification options such as K-means (Lu et al. 2018; Abdulridha et al. 2019) and the principal component analysis (Lu et al. 2018) were popular along with binary thresholds classifiers based on pixel values (Dammer et al. 2011). This thesis work yielded the best results when the adaptation of both machine learning for original classification of pixels is followed by binary threshold classification to correct misclassified pixels in the hemp model.

The gray mold on hemp case study, along with many of other studies attempting to detect fungal diseases, incorporated fungicide applications that create varying degrees of disease incidence and severity (Franke and Menz 2007; Heim et al. 2019). This allowed for nontreated plots, which were heavily infected with disease, and treated plots that contained little to no disease, and the collection of ground truth data. We found this to be very helpful in our hemp gray mold study because it allowed for not only the presence of diseased plants and non-diseased plants at a plot level which could be used in statistical analysis, but also provided the opportunity to compare remotely-sensed results with ground truth disease incidence and application of this work in an agricultural setting. West et al. (2003) acknowledges the potential benefits of optical sensors for fungal disease detection in targeted spray treatments, but mentions the likelihood of underestimating disease patch size, which was also found to be true in this study. Bravo et al. (2003) and Zhang et al. (2011) evaluated various plant cultivars with different levels of resistance

to create disease gradients, which enabled a similar type of analysis and illustrates an additional application of remote sensing.

The case study set explored in this thesis did discover limitations to this research and subsequent application of this technology. Because the lesions caused by *Leptosphaeria* on leaves of turnip and other brassicas are relatively small, optical sensors we had access to did not have the spatial resolution required for detection of black leg leaf spots on turnip for drone flights at 10 m and 20 m above ground level. Additional challenges arise when entire turnip plants are imaged *ex situ* rather than as individual leaves that are laid flat and imaged *in situ*. Field-like conditions, such as abiotic and biotic factors that influence the quality of image classification, will also increase the difficultly of remote sensing work. In gray mold on hemp, scaling up from a single acre to larger acreage may be difficult and would require increasingly long flight times and data storage space, among other factors. Models developed from this thesis work should be considered preliminary and could be ineffective when used in another field or region, thus requiring additional training data on a field-by-field basis until a sufficiently large data set is developed for the respective model. Additionally, these remote sensing methods are limited to data collected from a nadir perspective and lack the optical ability to detect disease found lower in the canopy, inside the canopy, or along the sides of the plant and flowering/non-flowering stems.

The future of agriculture is becoming more reliant on precision technology as agricultural land becomes more valuable and growing concerns over food security that must be addressed to meet increasing food demands experienced globally (Gebbers and Adamchuk 2010). Using these tools in agricultural contexts will accelerate the advancement this technology, making it more likely to be adopted by researchers and growers when given effective examples of its use. Future research needs include model optimization for correct characterization of healthy and diseased plant tissue as demonstrated by a high model accuracy, specificity, and sensitivity through a more robust training data set, inclusion of variables with a greater ability to distinguish between pixel classes, larger data sets, and alternative machine learning or

deep learning models. Additionally, to make remote sensing feasible for larger acreage field sites, image acquisition at heights greater than 1.5 m AGL are necessary even for diseases that present as relatively small leaf spots, such as black leg on turnip in this case study. While the number of studies reporting on detection of plant disease by remote sensing has increased over the past two decades, the methods utilized in these case studies, commonly applied in many others, should continue to be extended to alternative diseases on different crops. Furthermore, studies which have found success in detecting biotic or abiotic stresses should be conducted over multiple years, in multiple fields of the same crop, and incorporate larger portions of cropping regions to ensure the models' ability to effectively classify disease across a regional or national landscape scale.

Chapter 5: Conclusions

This thesis covering case studies on remote sensing and machine learning used for disease detection of black leg on turnip and gray mold on hemp addressed two objectives. First, this research aimed to understand if remote sensing coupled with machine learning could be used to detect these two diseases. Based on the results, remotely-sensed data can be used to train an SVM using the novel vegetation index, MGRVI, which allows for detection of gray mold on hemp. Additionally, an SVM model using NDVI and the red band as indicators of disease, allowed for accurate detection of black leg on turnip. While these accomplishments should not be overlooked, further research and analysis is necessary to validate the application of these tools in field-based settings and in a larger regional setting. Secondly, this work also addressed whether remote sensing and machine learning could be used as an alternative disease detection method to the traditional field-based technique of scouting on foot. This was accomplished in the hemp case study by utilizing a biofungicide trial set-up and comparing disease incidence ratings done on foot to remotely-sensed disease incidence findings that incorporated machine learning tools. This research found that gray mold incidence could be quantified with remotely-sensed data using an SVM model, but there are limitations to adopting as a replacement for traditional field scouting on foot. Results indicate this tool could be used as an alternative to field-based techniques if ranking the order of treatments is prioritized over the true percentage of disease incidence that would be found in the field on foot. In regard to the remote detection of black leg on turnip, results indicate that increased spatial resolution is needed for field-based applications of remote sensing technology along with further model development.

This research builds on recent studies that have successfully used remote sensing with multispectral sensors for detection of plant disease. Our work utilized similar methodological frameworks found in other studies conducting detection of plant disease via remote sensing and machine learning. Flights of hemp fields were

conducted at an average elevation comparable to other studies that accomplished disease detection with UAVs, while the black leg on turnip detection utilized a lower elevation and likely requires an optical sensor/camera with greater spatial resolution for the inclusion of a UAV for disease detection. Both case studies utilized vegetation indices with an SVM model for pixel-based classification of vegetation. The hemp model also incorporates a binary classifier threshold, which is less commonly used but still effective; present work gravitates towards integrated machine learning and more recently, deep learning models. For detection of gray mold on hemp, a real-world application for this research was utilized by comparing ground-based disease incidence rating with remote sensing model-based disease incidence ratings. Future work should demonstrate the application of remote sensing conducted *ex situ* to facilitate the adoption of these tools by growers and researchers. Furthermore, increasingly higher flight elevations, examination of a wider set of host-pathogen systems for remote disease assessment, and field-based detection in the presence of other abiotic and biotic factors should all be sought after as all are essential for the widespread adoption of remote disease detection.

Bibliography

Abbey, J. A., Percival, D., Abbey, L., Asiedu, S. K., Prithiviraj, B., and Schilder, A. 2019. Biofungicides as alternative to synthetic fungicide control of grey mould (*Botrytis cinerea*) - prospects and challenges. Biocontrol Sci Technol. 29:207-228.

Abdulridha, J., Ehsani, R., Abd-Elrahman, A., and Ampatzidis, Y. 2019. A remote sensing technique for detecting laurel wilt disease in avocado in presence of other biotic and abiotic stresses. Comput. Electron. Agric. 156:549-557.

Agostini, A., Johnson, D. A., Hulbert, S., Demoz, B., Fernando, W. G. D., and Paulitz, T. 2013. First report of blackleg caused by *Leptosphaeria maculans* on canola in Idaho. Plant Dis. 97:842-842.

Albetis, J., Duthoit, S., Guttler, F., Jacquin, A., Goulard, M., Poilvé, H., Feret, J-B., and Dedieu, G. 2017. Detection of Flavescence dorée grapevine disease using Unmanned Aerial Vehicle (UAV) multispectral imagery. Remote Sens. 9:308.

Anderson, J. P. 1924. *Botrytis cinerea* in Alaska. Phytopathology 14:152-155.

Anderson, L. C. 1974. A study of systematic wood anatomy in *Cannabis.* Botanical Museum Leaflets, Harvard University 24:29-36.

Araus, J. L., and Cairns, J. E. 2014. Field high-throughput phenotyping: the new crop breeding frontier. Trends Plant Sci. 19:52-61.

Arivazhagan, S., Shebiah, R. N., Ananthi, S., and Varthini, S. V. 2013. Detection of unhealthy region of plant leaves and classification of plant leaf diseases using texture features. Agric. Eng. Int.: CIGR Journal 15:211-217.

Astill, G., Perez, A., and Thornsbury, S. 2020. Developing Automation and Mechanization for Specialty Crops: A Review of US Department of Agriculture Programs: A Report to Congress, AP-082, U.S. Department of Agriculture, Economic Research.

Aylor, D. E. 1990. The role of intermittent wind in the dispersal of fungal pathogens. Annu. Rev. Phytopathol. 28:73-92.

Backhouse, D., and Willetts, H. J. 1984. A histochemical study of sclerotia of *Botrytis cinerea* and *Botrytis fabae*. Can. J. Microbiol. 30:171-178.

Balthazar, C., Cantin, G., Novinscak, A., Joly, D. L., and Filion, M. 2020. Expression of putative defense responses in *Cannabis* primed by *Pseudomonas* and/or *Bacillus* strains and infected by *Botrytis cinerea*. Front. Plant Sci. 11:1873.

Barbedo, J. G. A. 2013. Digital image processing techniques for detecting, quantifying and classifying plant diseases. SpringerPlus 2:1-12.

Barbedo, J. G. A. 2016. A review on the main challenges in automatic plant disease identification based on visible range images. Biosyst. Eng. 144:52-60.

Barbedo, J. G. A., Koenigkan, L. V., and Santos, T. T. 2016. Identifying multiple plant diseases using digital image processing. Biosyst. Eng. 147:104-116.

Barnes, E., Clarke, T. R., Richards, S. E., Colaizzi, P., Haberland, J., Kostrzewski, M., Waller, P., Choi, C., Riley, E., and Thompson, T. L. 2000. Coincident detection of crop water stress, nitrogen status, and canopy density using ground based multispectral data. On-line at https://naldc-legacy.nal.usda.gov/naldc/download.xhtml?id=4190&content=PDF.

Bates, T. A., Block, M. H., Wiseman, M. S., Garfinkel, A. R., Gent, D. H., and Ocamb, C. M. 2021a. First report of powdery mildew caused by *Podosphaera macularis* on hemp (*Cannabis sativa*) in Oregon. Plant Health Prog. 2021: *in press*.

Bates, T. A., Dietrich, M., and Ocamb, C. M. 2021b. Evaluation of bio-fungicides for gray mold on hemp in Oregon, 2021. Plant Disease Management Reports: Report No. 15:V048.

Behmann, J., Steinrücken, J., and Plümer, L. 2014. Detection of early plant stress responses in hyperspectral images. ISPRS J. Photogramm. Remote Sens. 93:98-111.

Berry, P. A. 2019. Decomposition of Brassicaceae Residue in the Willamette Valley. PhD Dissertation. Oregon State University, Corvallis, Oregon.

Biddulph, J. E., Fitt, B. D., Leech, P. K., Welham, S. J., and Gladders, P. 1999. Effects of temperature and wetness duration on infection of oilseed rape leaves by ascospores of *Leptosphaeria maculans* (stem canker). Eur. J. Plant Pathol. 105:769-781.

Bivand R., Keitt, T., and Rowlingson, B. 2020. rgdal: Bindings for the 'Geospatial' Data Abstraction Library. R package version 1.5-18. On-line at https://CRAN.R-project.org/package=rgdal.

Blanco, C., Los de Santos, B., and Romero, F. 2006. Relationship between concentrations of *Botrytis cinerea* conidia in air, environmental conditions, and the incidence of grey mould in strawberry flowers and fruits. Eur. J. Plant Pathol. 114:415-425.

Boddy, L. 2016. Pathogens of autotrophs. In: Watkinson, S. C., Money, N., and Boddy, L., editors. The Fungi. Academic Press; pages 245-292.

Bulger, M. A., Ellis, M. A., and Madden, L. V. 1987. Influence of temperature and wetness duration on infection of strawberry flowers by *Botrytis cinerea* and disease incidence of fruit originating from infected flowers. Phytopathology 77:1225-1230.

Bravo, C., Moshou, D., West, J., McCartney, A., and Ramon, H. 2003. Early disease detection in wheat fields using spectral reflectance. Biosyst. Eng. 84:137-145.

Breiman, L. 2001. Random forests. Mach. Learn. 45:5-32.

Broome, J. C., English, J. T., Marois, J. J., Latorre, B. A., and Aviles, J. C. 1995. Development of an infection model for *Botrytis* bunch rot of grapes based on wetness duration and temperature. Phytopathology 85:97-102.

Camargo, A., and Smith, J. S. 2009a. Image pattern classification for the identification of disease causing agents in plants. Comput. Electron. Agric. 66:121-125.

Camargo, A., and Smith, J. S. 2009b. An image-processing based algorithm to automatically identify plant disease visual symptoms. Biosyst. Eng. 102:9-21.

Candiago, S., Remondino, F., De Giglio, M., Dubbini, M., and Gattelli, M. 2015. Evaluating multispectral images and vegetation indices for precision farming applications from UAV images. Remote Sens. 7:4026-4047.

Cao, Q., Miao, Y., Wang, H., Huang, S., Cheng, S., Khosla, R., and Jiang, R. 2013. Non-destructive estimation of rice plant nitrogen status with Crop Circle multispectral active canopy sensor. Field Crops Res. 154:133-144.

Carisse, O. 2016. Epidemiology and aerobiology of *Botrytis* spp. In: Fillinger, S. and Elad, Y., editors. *Botrytis* - the Fungus, the Pathogen and its Management in Agricultural Systems. Springer; pages 127-148.

Carisse, O., Tremblay, D. M., and Lefebvre, A. 2015. Comparison of *Botrytis cinerea* airborne inoculum progress curves from raspberry, strawberry and grape plantings. Plant Pathol. 63:983-993.

Carisse, O., Tremblay, D. M., Lévesque, C. A., Gindro, K., Ward, P., and Houde, A. 2009. Development of a TaqMan real-time PCR assay for quantification of airborne conidia of *Botrytis squamosa* and management of Botrytis leaf blight of onion. Phytopathology 99:1273-1280.

Carus, M., and Sarmento, L. 2016. The European Hemp Industry: Cultivation, processing and applications for fibres, shivs, seeds and flowers. European Industrial Hemp Association 2016-05. 1-9. On-line at https://eiha.org/2016/05/.

Chandra, S., Lata, H,. Khan, I. A., and ElSohly, M. A. 2017. *Cannabis sativa* L.: botany and horticulture. In: Chandra, S., Lata, H., ElSohly, M. editors. *Cannabis sativa* L. - Botany and Biotechnology. Springer; pages 79-100.

Chen, J. M. 1996. Evaluation of vegetation indices and a modified simple ratio for boreal applications. Can. J. Remote. Sens. 22:229-242.

Cherney, J. H., and Small, E. 2016. Industrial hemp in North America: Production, politics and potential. Agronomy 6:58.

Claassen, B. J., Mallory-Smith, C., and Ocamb, C. M. 2015. Weeds as alternate hosts for fungal diseases of *Brassicas*. In: Western Society of Weed Science Annual Meeting Western Soc. of Weed Sci., Portland, OR, USA.

Claassen, B. J. 2016. Investigations of Black Leg and Light Leaf Spot on Brassicaceae Hosts in Oregon. MSc thesis, Oregon State University, Corvallis, Oregon.

Cohen, J. 1960. A coefficient of agreement for nominal scales. Educ. Psychol. Meas. 20:37-46.

Cohen, Y., Alchanatis, V., Zusman, Y., Dar, Z., Bonfil, D. J., Karnieli, A., and Shenker, M. 2010. Leaf nitrogen estimation in potato based on spectral data and on simulated bands of the VENμS satellite. Precis. Agric. 11:520-537.

Daberkow, S. G., and McBride, W. D. 2000. Adoption of precision agriculture technologies by US farmers. In: Proceedings of the 5th International Conference on Precision Agriculture, Bloomington, Minnesota, USA. Pages 1-12.

Daberkow, S. G., and McBride, W. D. 2003. Farm and operator characteristics affecting the awareness and adoption of precision agriculture technologies in the US. Precis. Agric. 4:163-177.

Dakshinamurti, C., Krishnamurthy, B., Summan-war, A. S., Shanta, P., and Pisharoty, P. R. 1971. Remote sensing for coconut wilt. In: Proceedings of 6th International Symposium on Remote Sensing of Environment. Environmental Research Institute at Michigan, Ann Arbor, USA. Pages 25-29.

Dammer, K. H., Möller, B., Rodemann, B., and Heppner, D. 2011. Detection of head blight (*Fusarium* ssp.) in winter wheat by color and multispectral image analyses. Crop Prot. 30:420-428.

Daponte, P., De Vito, L., Glielmo, L., Iannelli, L., Liuzza, D., Picariello, F., and Silano, G. 2019. A review on the use of drones for precision agriculture. IOP Conf. Ser.: Earth Environ. Sci. 275:012022.

Dean, R., Van Kan, J. A., Pretorius, Z. A., Hammond-Kosack, K. E., Di Pietro, A., Spanu, P. D., Rudd, J. J., Dickman, M., Kahmann, R., Ellis, J., and Foster, G. D. 2012. The Top 10 fungal pathogens in molecular plant pathology. Mol. Plant Pathol. 13:414-430.

De Gruyter, J., Woudenberg, J. H. C., Aveskamp, M. M., Verkley, G. J. M., Groenewald, J. Z., and Crous, P. W. 2013. Redisposition of Phoma-like anamorphs in *Pleosporales*. Stud. Mycol. 75:1-36.

De Kock, S. L., and Holz, G. 1992. Blossom-end rot of pears: Systemic infection of flowers and immature fruit by *Botrytis cinerea*. J. Phytopathol. 135:317-327.

Del Rio Mendoza, L. E., Nepal, A., and Markell, S. 2012. Outbreak of blackleg in canola in North Dakota is caused by new pathogenicity groups. Plant Health Prog. 13:19.

Dempsey, J. M. 1975. Fiber Crops. Univ. Presses of Florida. 470 pp.

Deng, L., Mao, Z., Li, X., Hu, Z., Duan, F., and Yan, Y. 2018. UAV-based multispectral remote sensing for precision agriculture: A comparison between different cameras. ISPRS J. Photogramm. Remote Sens. 146:124-136.

Dewey, L. 1913. Hemp Industry in America. US Department of Agriculture Yearbook 238.

Dilmaghani, A., Balesdent, M. H., Didier, J. P., Wu, C., Davey, J., Barbetti, M. J., Hua, L., Moreno-Rico, O., Phillips, D., Despeghel, J. P., Vincenot, L., Gout, L., and Rouxel, T. 2009. The *Leptosphaeria maculans-Leptosphaeria biglobosa* species complex in the American continent. Plant Pathol. 58:1044-1058.

Ehrensing, D. T. 1998. Feasibility of Industrial Hemp Production in the United States Pacific Northwest. Agricultural Experiment Station, Oregon State University Station Bulletin 681.

Elad, Y. 2016. Cultural and integrated control of *Botrytis* spp. In: Fillinger, S. and Elad, Y., editors. *Botrytis* - the Fungus, the Pathogen and its Management in Agricultural Systems. Springer; pages 149-164.

Elad, Y., Vivier, M., and Fillinger, S. 2016. *Botrytis*, the good, the bad and the ugly. In: Fillinger, S. and Elad, Y., editors. *Botrytis* - the Fungus, the Pathogen and its Management in Agricultural Systems. Springer; pages 1-15.

El-Helaly, A. F., Elarosi, H., Assawah, M. W., and Kilani, A. 1962. Studies on fungi associated with onion crop in the field and during storage. Phytopathologia Mediterranea 2:37-45.

Ellerbrock, L. A., and Lorbeer, J. W. 1977. Survival of sclerotia and conidia of *Botrytis squamosa*. Phytopathology 67:219-225.

Engelbrecht, R. 2002. The role of the Mediterranean fruit fly, *Ceratitis capitata*, in *Botrytis* bunch rot on grape. MSc thesis, University of Stellenbosch, Stellenbosch, South Africa.

Erickson, B., and Lowenberg-DeBoer, J. 2020. 2020 Precision Agriculture Dealership Survey. Purdue University. On-line at https://ag.purdue.edu/digital-ag-resources/wp-content/uploads/2020/11/CropLife-Report-2020.pdf.

EPA Pesticide Registration. 2021. Pesticide Products Registered for Use on Hemp. United States Environmental Protection Agency. On-line at https://www.epa.gov/pesticide-registration/pesticide-products-registered-use-hemp.

Epton, H. A. S., and Richmond, D. V. 1980. Formation, structure and germination of conidia. In: Jovanovich, B., Verhoeff, K., and Jarvis, W. R., editors. The Biology of *Botrytis*. Academic Press; pages 41-83.

Fairchild, D. S. 1988. Soil information system for farming by kind of soil. In: Proceedings, International Interactive Workshop on Soil Resources: Their Inventory, Analysis and Interpretations for Use in 1990's. Educational Development System, Minnesota Extension Service, University of Minnesota, St. Paul, Minnesota, USA; pages 159-164.

Farinas, C., and Peduto Hand, F. 2020. First report of *Golovinomyces spadiceus* causing powdery mildew on industrial hemp (*Cannabis sativa*) in Ohio. Plant Dis. 104:2727.

Farr, D.F., and Rossman, A.Y. Fungal Databases, U.S. National Fungus Collections, ARS, USDA. Retrieved April 21, 2021. https://nt.ars-grin.gov/fungaldatabases/.

Ferentinos, K. P. 2018. Deep learning models for plant disease detection and diagnosis. Comput. Electron. Agric. 145:311-318.

Ferentinos, K. P., Barda, M., and Damer, D. 2019. An Image-Based Deep Learning Model for Cannabis Diseases, Nutrient Deficiencies and Pests Identification. In: Oliveira, P. M., Novais, P., and Reis L. P., editors. EPIA Conference on Artificial Intelligence pages, Springer; pages 134-145.

Fitt, B. D. L., Creighton, N. F., and Bainbridge A. 1985. Role of wind and rain in dispersal of *Botrytis fabae* conidia. Trans. Br. Mycol. Soc. 85:307-312.

Fitt, B. D. L., Brun, H., Barbetti, M. J., and Rimmer, S. R. 2006. Worldwide importance of phoma stem canker (*Leptosphaeria maculans* and *Leptosphaeria biglobosa*) on oilseed rape (*Brassica napus*). Eur. J. Plant Pathol. 114:3-15.

Fortenbery, T. R., and Mick, T. B. 2014. Industrial hemp: opportunities and challenges for Washington. Washington State University Working Paper 2014-10. On-line at http://ses.wsu.edu/wp-content/uploads/2015/02/WP2014-10.pdf.

Fourie, J. F., and Holz, G. 1995. Initial infection processes by *Botrytis cinerea* on nectarine and plum fruit and the development of decay. Phytopathology 85:82-87.

Franke, J., and Menz, G. 2007. Multi-temporal wheat disease detection by multi-spectral remote sensing. Precis. Agric. 8:161-172.

Garcia-Ruiz, F., Sankaran, S., Maja, J. M., Lee, W. S., Rasmussen, J., and Ehsani, R. 2013. Comparison of two aerial imaging platforms for identification of Huanglongbing-infected citrus trees. Comput. Electron. Agric. 91:106-115.

Garfinkel, A. R. 2021. The history of *Botrytis* taxonomy, the rise of phylogenetics, and implications for species recognition. Phytopathology 111:437-454.

Gebbers, R., and Adamchuk, V. I. 2010. Precision agriculture and food security. Science 327:828-831.

Ghanbarnia, K., Dilantha Fernando, W. G., and Crow, G. 2011. Comparison of disease severity and incidence at different growth stages of naturally infected canola plants under field conditions by pycnidiospores of *Phoma lingam* as a main source of inoculum. Can. J. Plant Pathol. 33:355-363.

Gibson, K. 2006. Hemp in the British Isles. J. Industrial Hemp 11:57-67.

Gitelson, A. A., Kaufman, Y. J., and Merzlyak, M. N. 1996. Use of a green channel in remote sensing of global vegetation from EOS-MODIS. Remote Sens. Environ. 58:289-298.

Gitelson, A. A., Viña, A., Ciganda, V., Rundquist, D. C., and Arkebauer, T. J. 2005. Remote estimation of canopy chlorophyll content in crops. Geophys. Res. Lett. 32:L08403. doi:10.1029/2005GL022688.

Gladders, P., and Musa, T. M. 1980. Observations on the epidemiology of *Leptosphaeria macutans* stem canker in winter oilseed rape. Plant Pathol. 29: 28-37.

Gladders, P., Symonds, B. V., Hardwick, N. V., and Sansford, C. E. 1998. Opportunities to control canker (*Leptosphaeria maculans*) in winter oilseed rape by improved spray timing. Proceedings of Integrated Control in Oilseed Crops, Poznañ, Poland, 1997. Bulletin OILB/SROP 21(5):111-120.

Grand View Research. 2020. Precision Farming Market Size, Share & Trends Analysis Report By Offering, By Application (Yield Monitoring, Weather Tracking, Field Mapping, Crop Scouting), By Region, and Segment Forecasts, 2021 - 2028. On-line at https://www.grandviewresearch.com/industry-analysis/precision-farming-market.

Griffin, T. W., and Lowenberg-DeBoer, J. 2005. Worldwide adoption and profitability of precision agriculture Implications for Brazil. Revista de Politica Agricola 14:20-37.

Griffin, T. W., Shockley, J. M., and Mark, T. B. 2018. Economics of precision farming. In: Kent Shannon, D., Clay, D. E., and Kitchen, N. R., editors. Precision Agriculture Basics. American Society of Agronomy, Crop Science Society of America, and Soil Science Society of America; pages 221-230.

Guo, X. W., Fernando, W. G. D., and Entz, M. 2005. Effects of crop rotation and tillage on blackleg disease of canola. Can. J. Plant Pathol. 27:53-57.

Hall, R., Chigogora, J. L., and Phillips, L. G. 1996. Role of seedborne inoculum of *Leptosphaeria maculans* in development of blackleg on oilseed rape. Can. J. Plant Pathol. 18:35-42.

Han, H., Guo, X., and Yu, H. 2016. Variable selection using mean decrease accuracy and Mean Decrease Gini based on random forest. In: 7th IEEE International Conference on Software Engineering and Service Science; pages 219-224.

Hansen, Z., Bernard, E., Grant, J., Gwinn, K., Hale, F., Kelly, H., and Stewart, S. 2020. Hemp Disease and Pest Management. The University of Tennessee, Institute of Agriculture publication W916. On-line at https://extension.tennessee.edu/publications/Documents/W916.pdf.

Hamuda, E., Glavin, M., and Jones, E. 2016. A survey of image processing techniques for plant extraction and segmentation in the field. Comput. Electron. Agric. 125:184-199.

Harrison, J. G., and Lowe, R. 1987. Wind dispersal of conidia of *Botrytis* spp. pathogenic to *Vicia faba*. Plant Pathol. 36:5-15.

Hartsel, J. A., Eades, J., Hickory, B., and Makriyannis, A. 2016. *Cannabis sativa* and hemp. In: Gupta, R., editor. Nutraceuticals: Efficacy, Safety and Toxicity. Eslevier; pages 735-754.

Hearst, M. A., Dumais, S. T., Osuna, E., Platt, J., and Scholkopf, B. 1998. Support vector machines. IEEE Intell. Syst. 13:8-28.

Heim, R. H., Wright, I. J., Scarth, P., Carnegie, A. J., Taylor, D., and Oldeland, J. 2019. Multispectral, aerial disease detection for myrtle rust (*Austropuccinia psidii)* on a lemon myrtle plantation. Drones 3:25.

Hennebert, G. L. 1973. *Botrytis* and *Botrytis*-like genera. Persoonia - Mol. Phylogeny Evolution Fungi 7:183-204.

Hijmans, R. J. 2020. raster: Geographic Data Analysis and Modeling. R package version 3.3-13. On-line at https://CRAN.R-project.org/package=raster.

Holz, G., Coertze, S., and Williamson, B. 2007. The ecology of *Botrytis* on plant surfaces. In: Elad, Y., Williamson, B., Tudzynski, P., and Delen, N., editors. *Botrytis*: Biology, Pathology and Control. Springer; pages 9-27.

Howlett, B. J., Idnurm, A., and Pedras, M. S. C. 2001. *Leptosphaeria maculans*, the causal agent of blackleg disease of Brassicas. Fungal Genet. Biol. 33:1-14.

Hsieh, T. F., Huang, J. W., and Hsiang, T. 2001. Light and scanning electron microscopy studies on the infection of oriental lily leaves by *Botrytis elliptica*. Eur. J. Plant Pathol. 107:571-581.

Huang, Y-J., Fitt, B. D. L., Jedryczka, M., Dakowska, S., West, J. S., Gladders, P., Steed, J. M., and Li, Z-Q. 2005. Patterns of ascospore release in relation to phoma stem canker epidemiology in England (*Leptosphaeria maculans*) and Poland (*Leptosphaeria biglobosa*). Eur. J. Plant Pathol. 111:263-277.

Huete, A. R. 1988. A soil-adjusted vegetation index (SAVI). Remote. Sens. Environ. 25:295-309.

Hunt, E. R., Doraiswamy, P. C., McMurtrey, J. E., Daughtry, C. S. T., Perry, E. M., and Akhmedov, B. 2013. A visible band index for remote sensing leaf chlorophyll content at the canopy scale. International J. Appl. Earth Observation Geoinformation 21:103-112.

Inglis, D. A., du Toit, L. J., and Miller, T. W. 2013. Production of Brassica Seed Crops in Washington State: A Case Study on the Complexities of Coexistence. Washington State University Extension. On-line at https://mtvernon.wsu.edu/path_team/EM062E.pdf.

Jarvis, W. R. 1962a. The infection of strawberry and raspberry fruits by *Botrytis cinerea* Fr. Ann. Appl. Biol. 50:569-575.

Jarvis, W. R. 1962b. The dispersal of spores of *Botrytis cinerea* Fr. in a raspberry plantation. Trans. Br. Mycol. Soc. 45:549-559.

Jarvis, W. R. 1977. *Botryotinia* and *Botrytis* species: Taxonomy, Physiology and Pathogenicity-A Guide to the Literature. Canada Department of Agriculture. 195 pp.

Jarvis, W. R. 1980. Taxonomy. In: Jovanovich, B., Verhoeff, K., and Jarvis, W. R., editors. The Biology of *Botrytis*. Academic Press; pages 1-18.

Jeliazkov, V. D., Noller, J. S., Angima, S. D., Rondon, S. I., Roseberg, R. J., Summers, S., Jones, G., and Sikora, V. 2019. What is Industrial Hemp? Oregon State University Extension publication EM 9240.

Jiang, H. E., Li, X., Zhao, Y. X., Ferguson, D. K., Hueber, F., Bera, S., and Li, C. S. 2006. A new insight into *Cannabis sativa* (Cannabaceae) utilization from 2500-year-old Yanghai Tombs, Xinjiang, China. J. Ethnopharmacology 108:414-422.

Jiang, H., Wang, L., Merlin, M. D., Clarke, R. C., Pan, Y., Zhang, Y., and Ding, X. 2016. Ancient *Cannabis* burial shroud in a central Eurasian cemetery. Econ. Bot. 70:213-221.

Johnson, K. B., and Powelson, M. L. 1983. Analysis of spore dispersal gradients of *Botrytis cinerea* and gray mold disease gradients in snap beans. Phytopathology 73:741-746.

Johnson, P. 1999. Industrial hemp: A critical review of claimed potentials *for Cannabis sativa*. Tappi Journal 82:113-123.

Jones, G. 2020. Map of registered outdoor hemp acreage-August 2020. On-line at https://extension.oregonstate.edu/crop-production/hemp/map-registered-outdoor-hemp-acreage-august-2020.

Karst, M. 2013. UAVs in agriculture: Rules of the sky. Entira Insights. On-line at http://entira.net/news-insights/entira-insights/uavs-in-agriculturerules-of-the-sky/.

Khangura, R. K., and Barbetti, M. 2001. Prevalence of blackleg (*Leptosphaeria maculans*) on canola (*Brassica napus*) in Western Australia. Aust. J. Exp. Agric. 41:71-80.

Kraenzel, D. G., Petry, T. A., Nelson, B., Anderson, M. J., Mathern, D., and Todd, R. 1998. Industrial hemp as an alternative crop in North Dakota. North Dakota State University, The Institute for Natural Resources and Economic Development, Agricultural Economics Report No. 402. On-line at https://ageconsearch.umn.edu/record/23264/.

Kuhn, M. 2020. caret: Classification and Regression Training. R package version 6.0-86. On-line at https://CRAN.R-project.org/package=caret.

Kutcher, H. R., Fernando, W. G. D., Turkington, T. K., and McLaren, D. L. 2011. Best management practices for blackleg disease of canola. Prairie Soils Crops 4:122-134.

Lamb, D. W. 2000. The use of qualitative airborne multispectral imaging for managing agricultural crops - A case study in south-eastern Australia. Aust. J. Exp. Agric. 40:725-738.

Lambert, D. M., Lowenberg-DeBoer, J., Griffin, T. W., Peone, J., Payne, T., and Daberkow, S. G. 2004. Adoption, Profitability, and Making Better Use of Precision Farming Data. Purdue University, Dept. Ag. Econ. Staff Paper No. 04-06.

Lamey, H. A., and Hershman, D. E. 1993. Black leg of canola (*Brassica napus*) caused by *Leptosphaeria maculans* in North Dakota. Plant Dis. 77:1263.

Lelong, C. C., Burger, P., Jubelin, G., Roux, B., Labbé, S., and Baret, F. 2008. Assessment of unmanned aerial vehicles imagery for quantitative monitoring of wheat crop in small plots. Sensors 8:3557-3585.

Leroux, P. 2007. Chemical control of *Botrytis* and its resistance to chemical fungicides. In: Elad, Y., Williamson, B., Tudzynski, P., and Delen, N., editors. *Botrytis*: Biology, Pathology and Control. Springer; pages 195-222.

Li, H., Sivasithamparam, K., and Barbetti, M. J. 2007. Soilborne ascospores and pycnidiospores of *Leptosphaeria maculans* can contribute significantly to blackleg disease epidemiology in oilseed rape (*Brassica napus*) in Western Australia. Australasian Plant Pathol. 36:439-444.

Li, W., Dong, R., Fu, H., and Yu, L. 2019. Large-scale oil palm tree detection from high-resolution satellite images using two-stage convolutional neural networks. Remote Sens. 11:11.

Liaw, A., and Wiener, M. 2002. Classification and regression by randomForest. R News 2:18-22.

Lillesand, T., Kiefer, R. W., and Chipman, J. 2015. Concepts and foundations of remote sensing. In: Lillesand, T., Kiefer, R. W., and Chipman, J., editors. Remote Sensing and Image Interpretation, 7th ed. John Wiley & Sons; pages 1-84.

Louis, C., Girard, M., Kuhl, G., and Lopez-Ferber, M. 1996. Persistence of *Botrytis cinerea* in its vector *Drosophila melanogaster*. Phytopathology 86:934-939.

Lu, J., Ehsani, R., Shi, Y., de Castro, A. I., and Wang, S. 2018. Detection of multi-tomato leaf diseases (late blight, target and bacterial spots) in different stages by using a spectral-based sensor. Scientific Reports 8:1-11.

Lyu, D., Backer, R., Robinson, W. G., and Smith, D. L. 2019. Plant growth-promoting rhizobacteria for *Cannabis* production: Yield, cannabinoid profile and disease resistance. Front. Microbiol. 10:1761.

Macdonald, R. B. 1984. A summary of the history of the development of automated remote sensing for agricultural applications. IEEE Trans Geosci Remote Sens. 6:473-482.

Mahlein, A. K. 2016. Plant disease detection by imaging sensors-parallels and specific demands for precision agriculture and plant phenotyping. Plant Dis. 100:241-251.

Mahlein, A. K., Oerke, E. C., Steiner, U., and Dehne, H. W. 2012. Recent advances in sensing plant diseases for precision crop protection. Eur. J. Plant Pathol. 133:197-209.

Mahlein, A. K., Rumpf, T., Welke, P., Dehne, H. W., Plümer, L., Steiner, U., and Oerke, E. C. 2013. Development of spectral indices for detecting and identifying plant diseases. Remote Sens. Environ. 128:21-30.

Mahlein, A. K., Steiner, U., Dehne, H. W., and Oerke, E. C. 2010. Spectral signatures of sugar beet leaves for the detection and differentiation of diseases. Precis. Agric. 11:413-431.

Maniruzzaman, M., Rahman, M. J., Al-MehediHasan, M., Suri, H. S., Abedin, M. M., El-Baz, A., and Suri, J. S. 2018. Accurate diabetes risk stratification using machine learning: role of missing value and outliers. J. Med. Syst. 42:1-17.

Markell, S., del Rio, L., Halley, S., Mazurek, S., Mathew, F., and Lamey, A. 2008. Blackleg of canola. North Dakota State University Extension Service publication PP-1367. On-line at https://library.ndsu.edu/ir/bitstream/handle/10365/5289/pp1367.pdf?sequence=1.

Meyer, D., Dimitriadou, E., Hornik, K., Weingessel, A., and Leisch, F. 2020. e1071: Misc Functions of the Department of Statistics, Probability Theory Group (Formerly: E1071), TU Wien. R package version 1.7-4. On-line at https://CRAN.R-project.org/package=e1071.

McPartland, J. M. 1996. A review of *Cannabis* diseases. J. International Hemp Association 3:19-23.

McPartland, J. M. 2003. American Phytopathological Society Common Names of Plant Diseases: Diseases of Hemp. On-line at https://www.apsnet.org/edcenter/resources/commonnames/Pages/Hemp.aspx.

McPartland, J. M. 2017. *Cannabis sativa* and *Cannabis indica* versus "Sativa" and "Indica". In: Chandra, S., Lata, H., ElSohly, M. editors. *Cannabis sativa* L. - Botany and Biotechnology. Springer; pages 101-121.

McPartland, J. M. 2018. *Cannabis* systematics at the levels of family, genus, and species. Cannabis Cannabinoid Research 3:203-212.

McPartland, J. M., Clarke, R. C., and Watson, D. P. 2000. Hemp Diseases and Pests: Management and Biological Control. CABI Publishers, New York, NY. 251 pp.

McPartland, J. M., Hegman, W., and Long, T. 2019. *Cannabis* in Asia: Its center of origin and early cultivation, based on a synthesis of subfossil pollen and archaeobotanical studies. Veg. Hist. Archaeobot. 28:691-702.

Mendes-Pereira, E., Balesdent, M. H., Brun, H., and Rouxel, T. 2003. Molecular phylogeny of the *Leptosphaeria maculans-L. biglobosa* species complex. Mycological Research 107:1287-1304.

Mohanty, S. P., Hughes, D. P., and Salathé, M. 2016. Using deep learning for image-based plant disease detection. Front. Plant Sci. 7:1419.

Moore, G. K. 1979. What is a picture worth? A history of remote sensing. Hydrological Sciences Bulletin 24:477-485.

Mordor Intelligence. 2020. Agriculture Drones Market - Growth, Trends, Covid-19 Impact, and Forecasts (2021 - 2026). On-line at https://mordorintelligence.com/industry-reports/agriculture-drones-market.

Mutka, A. M., and Bart, R. S. 2015. Image-based phenotyping of plant disease symptoms. Front. Plant Sci. 5:734.

Naidu, R. A., Perry, E. M., Pierce, F. J., and Mekuria, T. 2009. The potential of spectral reflectance technique for the detection of Grapevine leafroll-associated virus-3 in two red-berried wine grape cultivars. Comput. Electron. Agric. 66:38-45.

Nair, N. G., and Nadtotchei, A. 1987. Sclerotia of *Botrytis* as a source of primary inoculum for bunch rot of grapes in New-South-Wales, Australia. J. Phytopathol. 119:42-51.

Nepal, A., Markell, S., Knodel, J., Bradley, C. A., and del Río Mendoza, L. E. 2014. Prevalence of blackleg and pathogenicity groups of *Leptosphaeria maculans* in North Dakota. Plant Dis. 98:328-335.

Nelson, R. E. 1951. Factors influencing the infection of table grapes by *Botrytis cinerea*. Phytopathology 41:319-326.

Neumann, M., Hallau, L., Klatt, B., Kersting, K., and Bauckhage, C. 2014. Erosion band features for cell phone image based plant disease classification. In: Proceedings of 22nd International Conference on Pattern Recognition. Stockholm, Sweden. Institute of Electrical and Electronics Engineers (IEEE), Piscataway, NJ; pages 3315-3320.

Nicot, P. C., Stewart, A., Bardin, M., and Elad, Y. 2016. Biological control and biopesticide suppression of *Botrytis*-incited diseases. In: Fillinger, S., and Elad, Y., editors. *Botrytis* - The Fungus, the Pathogen and its Management in Agricultural Systems. Springer; pages 165-187.

Ocamb, C. M., Mallory-Smith, C., Thomas, W. J., Serdani, M., and Putnam, M. L. 2015. New and re-emerging fungal pathogens affecting Brassicaceae plants in western Oregon: Black leg, light leaf spot, and white leaf spot. Phytopathology 105:542-P.

ODA. 2020. Oregon Department of Agriculture Public Comment on Hemp (Governor Brown's letter to the USDA secretary Sonny Perdue). On-line at https://www.oregon.gov/oda/programs/NurseryChristmasTree/Documents/Hemp/ODAPublicCommentHemp.pdf.

Olofsson, P., Foody, G. M., Herold, M., Stehman, S. V., Woodcock, C. E., and Wulder, M. A. 2014. Good practices for estimating area and assessing accuracy of land change. Remote Sens. Environ. 148:42-57.

Pârvu, M., and Pârvu, A. E. 2014. Parasitic fungi Sclerotiniaceae: Morphology and ultrastructure. In: Mendez-Vilas, editor. Microscopy: Advances in Scientific Research and Education. FORMATEX; pages 530-537.

Paulitz, T. C., Knerr, A. J., Carmody, S. M., Schlatter, D., Sowers, K., Derie, M. L., and du Toit, L. J. 2017. First report of *Leptosphaeria maculans* and *Leptosphaeria biglobosa*, causal agents of blackleg, on canola in Washington State. Plant Dis. 101:504.

Pierce, F. J., Anderson, N. W., Colvin, T. S., Schueller, J. K., Humburg, D. S., and McLaughlin, N. B. 1997. Yield mapping. In: Pierce, F. J., and Sadler, E. J., editors. The state of site specific management for agriculture. ASA, CSSA, and SSSA Books; pages 211-243.

Pontius Jr, R. G., and Millones, M. 2011. Death to Kappa: birth of quantity disagreement and allocation disagreement for accuracy assessment. Int. J. Remote Sens. 32:4407-4429.

Price, R. R., and Hummel, J. W. 1994. Soil organic matter content prediction using visible and near-infrared wavelengths. American Society of Agricultural Engineers Meeting (USA). No. 94-1039/94-1074.

Pscheidt, J. W., and Ocamb, C. M. 2021. Turnip and Rutabaga (*Brassica* sp.)-Black Leg (Phoma Dry Rot). In: Pscheidt, J. W., and Ocamb, C. M., editors. Pacific Northwest Plant Disease Management Handbook. On-line at https://pnwhandbooks.org/plantdisease/host-disease/turnip-rutabaga-brassica-sp-black-leg-phoma-dry-rot.

Punja, Z. K. 2018. Flower and foliage-infecting pathogens of marijuana (*Cannabis sativa* L.) plants. Can. J. Plant Pathol. 40:514-527.

Punja, Z. K. 2020a. Epidemiology of *Fusarium oxysporum* causing root and crown rot of cannabis (*Cannabis sativa* L., marijuana) plants in commercial greenhouse production. Can. J. Plant Pathol. DOI: 10.1080/07060661.2020.1788165.

Punja, Z. K. 2020b. First report of the hops powdery mildew pathogen, *Podosphaeria macularis*, on naturally infected marijuana (*Cannabis sativa* L.) plants in the field. Phytopathology 110:S2.10.

Punja, Z. K., Collyer, D., Scott, C., Lung, S., Holmes, J., and Sutton, D. 2019. Pathogens and molds affecting production and quality of *Cannabis sativa* L. Front. Plant Sci. 10:1120.

Punja, Z. K., Rodriguez, G., and Chen, S. 2017. Assessing Genetic Diversity in *Cannabis sativa* Using Molecular Approaches. In: Chandra, S., Lata, H., ElSohly, M. editors. *Cannabis sativa* L. - Botany and Biotechnology. Springer; pages 395-418.

Punja, Z. K., Scott, C., and Chen, S. 2018. Root and crown rot pathogens causing wilt symptoms on field-grown marijuana (*Cannabis sativa* L.) plants. Can. J. Plant Pathol. 40:528-541.

R Core Team. 2013. R: A language and environment for statistical computing. R Foundation for Statistical Computing. Vienna, Austria. On-line at http://www.R-project.org/.

Raman, V., Budel, J. M., Lata, H., Chandra, S., Khan, I. A., and ElSohly, M. A. 2019. Identification of *Cannabis sativa* using morpho-anatomy and microscopic characteristics. Conference paper from the XIIth Brazilian Symposium of Pharmacognosy and XVIIth Latin American Symposium on Pharmacobotany, Petrópolis, RJ, Brazil. On-line at https://www.researchgate.net/publication/333993017_Identification_of_Cannabis_sativa_using_morpho-anatomical_and_microscopic_characteristics.

Raman, V., Lata, H., Chandra, S., Khan, I. A., and ElSohly, M. A. 2017. Morpho-anatomy of marijuana (*Cannabis sativa* L.). In: Elad, Y., Williamson, B., Tudzynski, P., and Delen, N., editors. *Botrytis*: Biology, Pathology and Control. Springer; pages 123-136.

Ramcharan, A., Baranowski, K., McCloskey, P., Ahmed, B., Legg, J., and Hughes, D. P. 2017. Deep learning for image-based cassava disease detection. Front. Plant Sci. 8:1852.

Rimmer, S. R., and Van den Berg, C. G. J. 2007. Black leg (Phoma stem canker). In: Rimmer, S.R., Shattuck V. I., and Buchwaldt, L., editors. Compendium of *Brassica* Diseases. American Phytopathological Society, St. Paul, MN; pages 19-22.

Rondeaux, G., Steven, M., and Baret, F. 1996. Optimization of soil-adjusted vegetation indices. Remote Sens. Environ. 55:95-107.

Rossel, R. V., Walvoort, D. J. J., McBratney, A. B., Janik, L. J., and Skjemstad, J. O. 2006. Visible, near infrared, mid infrared or combined diffuse reflectance spectroscopy for simultaneous assessment of various soil properties. Geoderma. 131:59-75.

Rouse, J. W., Jr., Haas, R. H., Schell, J. A., and Deering, D. W. 1974. Monitoring Vegetation Systems in the Great Plains with ERTS. In: Third Earth Resources Technology Satellite Symposium, Washington, DC, 1973; pages 309-313.

Roussel, J. R., and Auty, D. 2020. Airborne LiDAR Data Manipulation and Visualization for Forestry Applications. R package version 3.0.4. On-line at https://cran.r-project.org/package=lidR.

Roussel, J. R., Auty, D., Coops, N. C., Tompalski, P., Goodbody, T. R. H., Sánchez Meador, A., Bourdon, J. F., De Boissieu, F., and Achim, A. 2020. lidR : An R package for analysis of Airborne Laser Scanning (ALS) data. Remote Sens. Environ. 251 (August), 112061. doi:10.1016/j.rse.2020.112061.

Rouxel, T., and Balesdent, M. H. 2005. The stem canker (blackleg) fungus, *Leptosphaeria maculans*, enters the genomic era. Mol. Plant Pathol. 6:225-241.

Rumpf, T., Mahlein, A. K., Steiner, U., Oerke, E. C., Dehne, H. W., and Plümer, L. 2010. Early detection and classification of plant diseases with support vector machines based on hyperspectral reflectance. Comput. Electron. Agric. 74:91-99.

Saleem, M. H., Potgieter, J., and Arif, K. M. 2019. Plant disease detection and classification by deep learning. Plants 8:468.

Sandino, J., Pegg, G., Gonzalez, F., and Smith, G. 2018. Aerial mapping of forests affected by pathogens using UAVs, hyperspectral sensors, and artificial intelligence. Sensors 18:944.

Sankaran, S., Mishra, A., Ehsani, R., and Davis, C. 2010. A review of advanced techniques for detecting plant diseases. Comput. Electron. Agric. 72:1-13.

Sankaran, S., Khot, L. R., Espinoza, C. Z., Jarolmasjed, S., Sathuvalli, V. R., Vandemark, G. J., and Pavek, M. J. 2015. Low-altitude, high-resolution aerial imaging systems for row and field crop phenotyping: A review. Eur. J. Agron. 70:112-123.

Sawler, J., Stout, J. M., Gardner, K. M., Hudson, D., Vidmar, J., Butler, L., and Myles, S. 2015. The genetic structure of marijuana and hemp. PLoS One 10:e0133292.

Seltenrich, N. 2019. Into the weeds: Regulating pesticides in *Cannabis*. Environ. Health Perspect. 127(4):on-line at https://doi.org/10.1289/EHP5265.

Seyb, A. M. 2003. *Botrytis cinerea* inoculum sources in the vineyard system. PhD Dissertation, Lincoln University, Lincoln, New Zealand.

Sexton, A. C., and Howlett, B. J. 2001. Green fluorescent protein as a reporter in the *Brassica-Leptosphaeria maculans* interaction. Physiol. Mol. Plant Pathol. 58:13-21.

Schimmelpfennig, D. 2016. Farm profits and adoption of precision agriculture. USDA, Economic Research Service, Economic Research Report Number 217.

Small, E., and Marcus, D. 2002. Hemp: A new crop with new uses for North America. In: J. Janick and A. Whipkey, editors. Trends in New Crops and New Uses. ASHS Press, Alexandria, VA; pages 284-326.

Smith, S. A. 2019. Industrial hemp: Economics and Marketing. University of Tennessee Extension, Institute of Agriculture. PowerPoint presentation on-line at https://extension.tennessee.edu/Rutherford/Documents/Hemp%202019-sas.pdf.

Sprague, S. J., Watt, M., Kirkegaard, J. A., and Howlett, B. J. 2007. Pathways of infection of *Brassica napus* roots by *Leptosphaeria maculans*. New Phytol. 176:211-222.

Stafford, J. V., and Miller, P. C. H. 1993. Spatially selective application of herbicide to cereal crops. Comput. Electron. Agric. 9:217-229.

Stafford, J. V. 2000. Implementing precision agriculture in the 21st century. J. Agric. Eng. 76:267-275.

Stehr, N. J. 2015. Drones: The newest technology for precision agriculture. Natural Sciences Education 44:89-91.

Szarka, D., Tymon, L., Amsden, B., Dixon, E., Judy, J., and Gauthier, N. 2019. First report of powdery mildew caused by *Golovinomyces spadiceus* on industrial hemp (*Cannabis sativa*) in Kentucky. Plant Dis. 103:1773-1773.

Taghinasab, M., and Jabaji, S. 2020. *Cannabis* microbiome and the role of endophytes in modulating the production of secondary metabolites: An overview. Microorganisms 8:355.

Thiessen, L. D., Schappe, T., Cochran, S., Hicks, K., and Post, A. R. 2020. Surveying for potential diseases and abiotic disorders of industrial hemp (*Cannabis sativa*) production. Plant Health Prog. 21:321-332.

Thomas, A. C., Kotze, J. M., and Matthee, F. N. 1983 Development of a technique for the recovery of soilborne sclerotia of *Botrytis cinerea*. Phytopathology 73:1374-1376.

Thomas, S., Kuska, M. T., Bohnenkamp, D., Brugger, A., Alisaac, E., Wahabzada, M., and Mahlein, A. K. 2018. Benefits of hyperspectral imaging for plant disease detection and plant protection: a technical perspective. J. Plant. Dis. Prot. 125:5-20.

Trimble Agriculture. 2021. Top 10 Agriculture Trends to Watch in 2021. On-line at https://agriculture.trimble.com/blog/top-10-agriculture-trends-to-watch-in-2021/?utm_content=152744281&utm_medium=social&utm_source=linkedin&hss_channel=lcp-9366145.

Tucker, C. J. 1979. Red and photographic infrared linear combinations for monitoring vegetation. Remote Sens. Environ. 8:127-150.

USDA AMS (USDA Agricultural Marketing Service). 2020. Hemp Production. On-line at https://www.ams.usda.gov/rules-regulations/hemp.

USDA ARMS (USDA Agricultural Resource Management Survey). 2010. Crop production practices (Subject: Corn and Soybean). On-line at https://data.ers.usda.gov/reports.aspx?ID=17883.

USDA ERS (USDA Economic Research Service). 2000. Industrial Hemp in the United States: Status and Market Potential. On-line at https://www.ers.usda.gov/webdocs/publications/41740/15867_ages001e_1_.pdf?v=8787.5.

USDA FSA (USDA Farm Service Agency). Crop Acreage Data. 2020. On-line at https://www.fsa.usda.gov/news-room/efoia/electronic-reading-room/frequently-requested-information/crop-acreage-data/index.

Urbasch, I. 1983. On the genesis and germination of the chlamydospores of *Botrytis cinerea* Pers. J. Phytopathol. 108:54-60.

Urbasch, I. 1986. *In vivo*-investigations on the formation and function of chlamydospores of *Botrytis cinerea* Pers. in the host-parasite-system *Fuchsia hybrida-B. cinerea*. J. Phytopathol. 117:276-282.

Veroustraete, F. 2015. The rise of the drones in agriculture. ECromicon Agriculture 2.2:325-327.

Vigneau, N., Ecarnot, M., Rabatel, G., and Roumet, P. 2011. Potential of field hyperspectral imaging as a non destructive method to assess leaf nitrogen content in wheat. Field Crops Res. 122:25-31.

Walker, A. S. 2016. Diversity within and between species of *Botrytis*. In: Fillinger, S., and Elad, Y., editors. *Botrytis* - The Fungus, the Pathogen and its Management in Agricultural Systems. Springer; pages 91-126.

Walsh, M. K., Whitlock, C., and Bartlein, P. J. 2010. 1200 years of fire and vegetation history in the Willamette Valley, Oregon and Washington, reconstructed using high-resolution macroscopic charcoal and pollen analysis. Palaeogeogr. Palaeoclimatol. Palaeoecol. 297:273-289.

West, J. S., Biddulph, J. E., Fitt, B. D., and Gladders, P. 1999. Epidemiology of *Leptosphaeria maculans* in relation to forecasting stem canker severity on winter oilseed rape in the UK. Ann. App. Biol. 135:535-546.

West, J. S., Bravo, C., Oberti, R., Lemaire, D., Moshou, D., and McCartney, H. A. 2003. The potential of optical canopy measurement for targeted control of field crop diseases. Annu. Rev. Phytopathol. 41:593-614.

West, J. S., Kharbanda, P. D., Barbetti, M. J., and Fitt, B. D. L. 2001. Epidemiology and management of *Leptosphaeria maculans* (Phoma stem canker) on oilseed rape in Australia, Canada and Europe. Plant Pathol. 50:10-27.

West, J. S., Liu, S., Evans, N., Hu, B., and Peng, L. 2000. *Leptosphaeria maculans* causing stem canker of oilseed rape in China. New Disease Reports 1:3.

Wing, M. G., Burnett, J., Johnson, S., Akay, A. E., and Sessions, J. 2014. A low-cost unmanned aerial system for remote sensing of forested landscapes. Int. J. Remote Sens. 4:113-120.

Winterhalter, L., Mistele, B., Jampatong, S., and Schmidhalter, U. 2011. High throughput phenotyping of canopy water mass and canopy temperature in well-watered and drought stressed tropical maize hybrids in the vegetative stage. Eur. J. Agron. 35:22-32.

Wiseman, M. S., Bates, T., Garfinkel, A., Ocamb, C. M., and Gent, D. H. 2021. First report of powdery mildew caused by *Golovinomyces ambrosiae* on *Cannabis sativa* in Oregon. Plant Dis. 105: on-line at https://doi.org/10.1094/PDIS-11-20-2455-PDN.

Wright, A. H. 1918. Wisconsin's hemp industry. Agricultural Experiment Station of the University of Wisconsin. Bulletin 293. On-line at https://hempology.org/ALL%20HISTORY%20ARTICLES.HTML/1918;WISCONSIN%20HEMP%20BUL293.html.

Yang, C. M., Cheng, C. H., and Chen, R. K. 2007. Changes in spectral characteristics of rice canopy infested with brown planthopper and leaffolder. Crop Sci. 47:329-335.

Zhang, J., Huang, Y., Pu, R., Gonzalez-Moreno, P., Yuan, L., Wu, K., and Huang, W. 2019. Monitoring plant diseases and pests through remote sensing technology: A review. Comput. Electron. Agric. 165:104943.

Zhang, W., Qi, J., Wan, P., Wang, H., Xie, D., Wang, X., and Yan, G. 2016. An easy-to-use airborne LiDAR data filtering method based on cloth simulation. Remote Sens. 8:501.

Zhang, N., Wang, M., and Wang, N. 2002. Precision agriculture - a worldwide overview. Comput. Electron. Agric. 36:113-132.

Zhou, R., Kaneko, S. I., Tanaka, F., Kayamori, M., and Shimizu, M. 2014. Disease detection of Cercospora leaf spot in sugar beet by robust template matching. Comput. Electron. Agric. 108:58-70.